



# 1 Measurement report: Regional characteristics of seasonal and long- 2 term variations in greenhouse gases at Nainital, India and Comilla, 3 Bangladesh

4 Shohei Nomura<sup>1</sup>, Manish Naja<sup>2</sup>, Md. Kawser Ahmed<sup>3</sup>, Hitoshi Mukai<sup>1</sup>, Yukio Terao<sup>1</sup>, Toshinobu  
5 Machida<sup>1</sup>, Motoki Sasakawa<sup>1</sup>, Prabir K. Patra<sup>4</sup>

6 <sup>1</sup>Center for Global Environmental Research, National Institute for Environmental Studies, 16-2 Onogawa, Tsukuba, Ibaraki,  
7 305-8506, Japan

8 <sup>2</sup>Aryabhatta Research Institute of Observational Sciences, Manora Peak, Nainital Uttarakhand 263129, India

9 <sup>3</sup>Department of Oceanography, Faculty of Earth & Environmental Sciences, University of Dhaka, Dhaka-1000, Bangladesh

10 <sup>4</sup>Research Institute for Global Change, JAMSTEC, 3173-25 Showa-machi, Yokohama, 236-0001, Japan

11 *Correspondence to:* Shohei Nomura (nomura.shohei@nies.go.jp) Tel.: +81 298502370; fax: +81 298502960

## 12 Abstract

13 Emissions of greenhouse gases (GHGs) from the Indian subcontinent have increased during the last 20 years along with  
14 rapid economic growth, however, there remains a paucity of GHG measurements for policy relevant research. In northern  
15 India and Bangladesh, agricultural activities are considered to play an important role on GHGs concentrations in the  
16 atmosphere. We performed weekly air sampling at Nainital (NTL) in northern India and Comilla (CLA) in Bangladesh from  
17 2006 and 2012, respectively. Air samples were analyzed for dry-air gas mole fractions of CO<sub>2</sub>, CH<sub>4</sub>, CO, H<sub>2</sub>, N<sub>2</sub>O, and SF<sub>6</sub>,  
18 and carbon and oxygen isotopic ratios of CO<sub>2</sub> ( $\delta^{13}\text{C-CO}_2$  and  $\delta^{18}\text{O-CO}_2$ ). Regional characteristics of these components over  
19 the Indo-Gangetic Plain are discussed compared to data from other Indian sites and Mauna Loa, Hawaii (MLO), which is  
20 representative of marine background air.

21 We found that the CO<sub>2</sub> mole fraction at both NTL and CLA had two seasonal minima in February–March and September,  
22 corresponding to crop cultivation activities that depend on regional climatic conditions. The carbon isotopic signature also  
23 suggested that photosynthetic CO<sub>2</sub> absorption by crops cultivated in each season contributes differently to lower CO<sub>2</sub> mole  
24 fractions. The CH<sub>4</sub> mole fraction of NTL and CLA in August–October showed high values (i.e., sometimes over 4,000 ppb at  
25 CLA) due to the influence of CH<sub>4</sub> emissions from the paddy fields in addition to the other sources due to the hot and humid  
26 climatic conditions. High CH<sub>4</sub> mole fractions sustained over months at CLA were a characteristic feature in the Indo-Gangetic  
27 Plain. The CO mole fractions at NTL were also high and showed peaks in May and October, while CLA had much higher  
28 peaks in October–March due to the influence of human activities such as emissions from biomass burning and brick production.  
29 The N<sub>2</sub>O mole fractions at NTL and CLA increased in June–August and November–February, which coincided with the  
30 application of nitrogen fertilizer and the burning of biomass such as the harvest residues and dung for domestic cooking. Based  
31 on H<sub>2</sub> seasonal variation at both sites, it appeared that the emissions in this region were related to biomass burning in addition  
32 to production from the reaction of OH and CH<sub>4</sub>. The SF<sub>6</sub> mole fraction was similar to that at MLO, suggesting that there were  
33 few anthropogenic emission sources in the district.

34 The variability of CO<sub>2</sub> growth rate at NTL was different from the variability in the CO<sub>2</sub> growth rate at MLO, which is  
35 more closely linked with the El Niño Southern Oscillation (ENSO). In addition, the growth rates of the CH<sub>4</sub> and SF<sub>6</sub> mole  
36 fractions at NTL showed an anticorrelation with those at MLO, indicating that the frequency of southerly air masses strongly  
37 influenced these mole fractions. These finding showed that rather large regional climatic conditions considerably controlled  
38 interannual variations in GHGs,  $\delta^{13}\text{C-CO}_2$ , and  $\delta^{18}\text{O-CO}_2$  through changes in precipitation and air mass.



## 39 Keywords

40 Northern India, Bangladesh, Greenhouse gases variation, Isotope ratio of CO<sub>2</sub>, Local emissions

## 41 1 Introduction

42 The atmospheric mole fractions of CO<sub>2</sub>, CH<sub>4</sub>, N<sub>2</sub>O and many other greenhouse gases (GHGs) are increasing until the  
43 recent years globally. As for CO<sub>2</sub>, rapid increases in CO<sub>2</sub> emissions from emerging countries contribute strongly to acceleration  
44 of the growth rate of its mole fraction (Friedlingstein et al., 2019). For instance, anthropogenic CO<sub>2</sub> emission of India has  
45 increased in 2017 it reached to 2.45 GtCO<sub>2</sub> yr<sup>-1</sup> which was the third highest in the world (Muntean et al., 2018). Therefore,  
46 South Asian region must be important to evaluate GHG in the future. Patra et al. (2013) calculated the CO<sub>2</sub> flux in South Asia  
47 using top-down and bottom-up methods and reported that CO<sub>2</sub> fluxes in top-down and bottom-up were  $-104 \pm 150$  TgCyr<sup>-1</sup>  
48 and  $-191 \pm 193$  TgCyr<sup>-1</sup>. In other words, CO<sub>2</sub> was absorbed in South Asia, however, the error of CO<sub>2</sub> flux was very large  
49 because there are few measured GHG moles fractions in the South Asian region.

50 Several observations on GHGs mole fractions in the atmosphere have been done around India. The first systematic  
51 monitoring for GHGs mole fractions and carbon isotopic ratio in the South Asian region was performed by Bhattacharya et al.  
52 (2009). They carried out monitoring at Cape Rama station (CRI) (15.1°N, 73.9°E, 60 m a.s.l.) on the West Coast of India from  
53 1993 and found that (1) the CH<sub>4</sub> and CO mole fractions increased in October–March when the air mass came from the northeast  
54 (inland), and decreased in June–August when the air mass came from southwest (ocean); (2) the CO<sub>2</sub>, CH<sub>4</sub>, CO, H<sub>2</sub> and N<sub>2</sub>O  
55 mole fractions in June–August were generally at the same levels at the background sites at the observatory in Seychelles Island  
56 and Hawaii Island; (3) the seasonal cycle and phase in CH<sub>4</sub> and CO mole fractions were quite similar and their correlation  
57 coefficient was high, generally because they originated from anthropogenic emissions in India. Therefore, it became clear that  
58 GHG mole fractions are greatly changed by the seasonal wind and that the Indian subcontinent has strong CH<sub>4</sub> and CO  
59 emissions (Patra et al., 2009).

60 In recent decades, a few more research groups have commenced flask sampling or continuous GHG measurements in  
61 India. Sharma et al. (2013) measured atmospheric CO<sub>2</sub> mole fractions at Dehradun in northern India in 2009 and detected that  
62 the CO<sub>2</sub> mole fraction decreased twice a year (March and September) due to vegetation activity. Ganesan et al. (2013) measured  
63 the CH<sub>4</sub>, N<sub>2</sub>O, and SF<sub>6</sub> mole fractions in December 2011 to February 2013 at Darjeeling in northeastern India and found that  
64 (1) CH<sub>4</sub> mole fractions had a positive correlation with the N<sub>2</sub>O mole fraction, and that those mole fractions increased due to  
65 emissions from anthropogenic activities when air masses came from the Indo-Gangetic Plain; (2) SF<sub>6</sub> emissions in the region  
66 showed a weak signal. Chandra et al. (2016) measured the CO<sub>2</sub> and CO mole fractions at Ahmedabad in western India and  
67 detected a decrease in the mole fraction when the air mass comes from southwest (ocean) and an increase in the mole fraction  
68 when the air mass comes from northeast (inland). Tiwari et al. (2014) analyzed the spatial variability of atmospheric CO<sub>2</sub> mole  
69 fractions using models over the Indian subcontinent and began the flask sampling at Sinhagad in western Ghats. They showed  
70 (1) the seasonal variation of the CO<sub>2</sub> mole fraction in southern India differed with the variation on the Indo-Gangetic Plain in  
71 northern India due to the differences in air mass transportation and anthropogenic activity; (2) the CO<sub>2</sub> mole fraction in July–  
72 October at Sinhagad was lower than the mole fraction of CRI on the west coast India because of the influence of photosynthesis  
73 by the regional forest ecosystem.

74 Sreenivas et al. (2016) measured the mole fractions of CO<sub>2</sub> and CH<sub>4</sub> at Shadnagar in central India and reported that the  
75 CO<sub>2</sub> and CH<sub>4</sub> mole fractions were strongly positively correlated to anthropogenic sources. Lin et al. (2015) commenced the  
76 most ambitious flask sampling network, with sites at Pondicherry (PON) on the southeast coast India, Port Blair (PBL) on  
77 Andaman Island, and Hanle (HLE) in northwestern Himalaya. They reported that (1) the mole fractions of CH<sub>4</sub>, CO, and N<sub>2</sub>O  
78 at PON and PBL were relatively high in comparison with those at HLE; (2) seasonal variations in GHGs at PON and PBL  
79 were quite different from the variation at HLE because the former two sites were exposed to the influence of air masses



80 originating from areas of anthropogenic activities. In addition to these studies at ground sites, recently aircraft-base  
 81 observations over Indo-Gangetic Plain such as CONTRAIL have been also carried out actively, evaluating seasonal variation  
 82 of CO<sub>2</sub> mole fraction (Umezawa et al, 2016).

83 Thus, the GHG observation program in Indian region is expanding gradually, however, observation sites and  
 84 characterization of GHG behavior and their long-term trends remain limited. In this work, we present an analysis of long record  
 85 (14 years) of various GHGs mole fraction and isotopic ratios of CO<sub>2</sub> ( $\delta^{13}\text{C}$ -CO<sub>2</sub> and  $\delta^{18}\text{O}$ -CO<sub>2</sub>) at Nainital, India on a mountain  
 86 site near the Himalayan mountain range, which can be considered as a background site representing Northern Indian air, and  
 87 which is partly influenced by anthropogenic activities from the Indo-Gangetic Plain. We also show a similar 8-year GHG  
 88 record at Comilla, Bangladesh located in the eastern edge of Indo-Gangetic Plain, where agricultural activities are believed to  
 89 the main factors for GHG emissions. The levels and seasonal variabilities of GHGs mole fraction at these sites are discussed  
 90 compared to those at other Indian sites reported previously, along with the local precipitation and 72 hr back trajectory to  
 91 summarize the behavior of GHGs in this region. Relationship of mole fractions among GHGs are evaluated. We also describe  
 92 isotopic characteristics of CO<sub>2</sub> to consider contribution on absorption by C<sub>3</sub> and C<sub>4</sub> plants in each region. Furthermore, we  
 93 analyze the relationships between the interannual variabilities in GHG growth rates and regional climatic condition such as the  
 94 Indian Dipole Mode Index (DMI) and the El Niño Southern Oscillation (ENSO) index.

## 95 2 Methods

### 96 2.1 Location

97 Figure 1 shows the locations of Nainital station (NTL) and Comilla station (CLA) where we performed weekly sampling.  
 98 The GHG observation sites in previous studies on the Indian subcontinent are also marked.

99 NTL is located at Aryabhata Research Institute of Observational Sciences (ARIES) (29.36°N, 79.46°E, 1940 m a.s.l.)  
 100 on the top of Mt. Mauna Peak on the foot of the Himalaya mountain range facing the Indo-Gangetic Plain. Also, NTL is located  
 101 3 km south of Nainital city and no local residential building within 2 km from the station. Predominant wind direction at NTL  
 102 show the west-northwest during winter and east during summer (Naja et al., 2016), which mean that NTL might be influenced  
 103 mainly by the air mass passing through the Indo-Gangetic Plain. We estimated that the air of NTL is not strongly influenced  
 104 by local GHGs emissions nearby.

105 CLA is located at Comilla weather station of Bangladesh Meteorological Department (BMD) (23.43°N, 91.18°E, 30 m  
 106 a.s.l.) on the edge of farming village with a flat landscape in central Bangladesh. The surrounding area of CLA cover the paddy  
 107 fields and a few farmhouses. Farmers in Comilla burn the biomass (e.g. harvest residuals, firewood and dung) on daily basis  
 108 and it was expected that CO<sub>2</sub>, CH<sub>4</sub>, CO, H<sub>2</sub>, N<sub>2</sub>O were emitted by the burning. CLA is considered to capture mainly the effect  
 109 of emission and sink in rural areas in eastern Indo-Gangetic Plain but may also capture some effect from nearby emissions.

### 110 2.2 Air sampling

111 Flask samples were collected from September 2006 in NTL and from June 2012 in CLA. Inlets were mounted at 7 m  
 112 above ground level (on the roof of the second floor of the station) in NTL and 8 m above ground level (on top of the 5 m tower  
 113 on the roof of the one-storey weather station building) in CLA. Air samples were collected in 1.5-L Pyrex flask through the  
 114 sampling line (Fig. 2[a]) at 2 p.m. (local time) once a week (usually on Wednesday). The sampling line contained a diaphragm  
 115 pump (MOA-P108-HB, GAST Co., Ltd.) and a freezer (VA-120, Taitec Co., Ltd.) for dehumidification by a glass trap. The  
 116 sampling flow rate was approximately 2 L min<sup>-1</sup> and the sample was passed through a -30 °C cooler and pressurized to 0.25  
 117 MPa after 10 min flushing through the sampling tube and flask. The sampled flasks were packed in a cardboard box and  
 118 transported to the laboratory of the Center for Global Environmental Research (CGER), National Institute for Environmental  
 119 studies, Japan (NIES) (transportation period: 3–7 days) for analyses.



## 120 2.3 Measurement methods

121 Air sample was passed through a -80 °C cold trap for dehumidification and was delivered to each instrument with a  
122 flow rate of 40 ml/min (see the analysis line in Fig. 2[b]). A nondispersive infrared analyser (NDIR; LI-COR, LI-6252) was  
123 used for CO<sub>2</sub> analysis, a gas chromatograph equipped with a flame ionization detector (GC-FID; Agilent Technologies, HP-  
124 5890 or HP-7890) was used to analyze CH<sub>4</sub>, a gas chromatograph with a reduction gas detector (GC-RGD; Agilent  
125 Technologies, HP-5890+Trace Analytical RGD-2 or Peak Laboratories, Peak Performer 1 RCP) was used for CO and H<sub>2</sub>  
126 analyses, and a gas chromatograph with an electron capture detector or a micro electron capture detector (GC-ECD or GC-  
127 micro-ECD; Agilent Technologies, HP-6890) was used to analyze N<sub>2</sub>O and SF<sub>6</sub>.

128 Dry-air mole fractions were measured against each of their working standard gases which were calibrated with NIES  
129 secondary standard gas series (CO<sub>2</sub>-NIES09 scale, CH<sub>4</sub>-NIES94 scale, CO-NIES09 scale, H<sub>2</sub>-NIES96 scale, N<sub>2</sub>O-NIES01  
130 scale, and SF<sub>6</sub>-NIES01 scale). Comparison between those scales and the National Oceanic and Atmospheric Administration  
131 (NOAA) scale in the 6<sup>th</sup> Round Robin intercomparison (NOAA/ESRL, 2019a) showed -0.04 to -0.09 ppm for CO<sub>2</sub>, 3.7 to 4.1  
132 ppb for CH<sub>4</sub>, 4.0 to 4.4 ppb for CO, -0.61 to -0.69 for N<sub>2</sub>O, and -0.03 to -0.06 ppt for SF<sub>6</sub>. We evaluated that the NIES scales  
133 were almost the same as NOAA scales except for CH<sub>4</sub> which showed a bias that was beyond the measurement precision of our  
134 instrument.

135 After the mole fraction analysis, we used the remaining air inside the flask for analysis of  $\delta^{13}\text{C-CO}_2$  and  $\delta^{18}\text{O-CO}_2$ . The  
136 air was introduced into two traps sequentially (-100 °C and -197 °C), which trapped H<sub>2</sub>O and CO<sub>2</sub>, respectively. Finally, CO<sub>2</sub>  
137 was sealed in a glass tube. Air  $\delta^{13}\text{C-CO}_2$  and  $\delta^{18}\text{O-CO}_2$  were measured using the working standard CO<sub>2</sub> gas which was prepared  
138 in our laboratory by MT-252. The method for producing the working standard gas is similar to the method for producing the  
139 NIES Atmospheric Reference CO<sub>2</sub> for Isotopic Studies (NARCIS), which is used for interlaboratory-scale comparison (Mukai,  
140 2001). The working standard scales of  $\delta^{13}\text{C-CO}_2$  and  $\delta^{18}\text{O-CO}_2$  are the same as those of NARCIS, which were measured by  
141 various institutions related to the World Meteorological Organization (WMO) (Mukai, 2003). The differences between NIES  
142 scales and INSTAAR (Institute of Arctic and Alpine Research) scales were 0.013–0.039‰ in the mean value range of -8.683  
143 to -8.759‰ for  $\delta^{13}\text{C-CO}_2$ , and -0.017–0.022‰ in the mean value range of -1.956 to -9.299‰ of  $\delta^{18}\text{O-CO}_2$  in the 6<sup>th</sup> Round  
144 Robin intercomparison (NOAA/ESRL, 2019a). The  $\delta^{18}\text{O-CO}_2$  for atmospheric CO<sub>2</sub> in this study is expressed against the value  
145 of CO<sub>2</sub> evolved from VPDB calcite (i.e., VPDB-CO<sub>2</sub> scale, [IAEA, 1993, Brand et al., 2010]). Although the VSMOW scale is  
146 often used for  $\delta^{18}\text{O}$  values of water, CO<sub>2</sub> evolved from VPDB calcite (VPDB-CO<sub>2</sub> scale) has similar  $\delta^{18}\text{O}$  values of CO<sub>2</sub>  
147 equilibrated with VSMOW water, which is the reference gas of the VSMOW scale. The difference between them is only  
148 0.263‰ (IAEA, 1993, Kim et al., 2015). Additionally, corrections for N<sub>2</sub>O bias and  $\delta^{17}\text{O-CO}_2$  showed by Brand et al. (2010)  
149 were made to obtain final isotope ratios.

## 150 2.4 Reference dataset

151 For comparison with the data of NTL and CLA, we obtained weekly data (CO<sub>2</sub>, CH<sub>4</sub>, CO, N<sub>2</sub>O, SF<sub>6</sub>,  $\delta^{13}\text{C-CO}_2$ , and  
152  $\delta^{18}\text{O-CO}_2$ ) from the Mauna Loa Observatory (MLO) (19.54°N, 155.58°W, 3397 m a.s.l.) on the NOAA/ESRL website  
153 (NOAA/ESRL, 2019b). We also used biweekly data for CO<sub>2</sub>, CH<sub>4</sub>, CO, H<sub>2</sub>, N<sub>2</sub>O, and  $\delta^{13}\text{C-CO}_2$  from Cape Rama, India (CRI)  
154 (15.08°N, 73.83°W, 60 m a.s.l.) on the website of World Data Centre for Greenhouse Gases (WDCGG) (WDCGG, 2017). The  
155 trends of mole fractions of CO<sub>2</sub>, CH<sub>4</sub>, CO, H<sub>2</sub>, N<sub>2</sub>O, and SF<sub>6</sub> and the isotopic ratio of  $\delta^{13}\text{C-CO}_2$  and  $\delta^{18}\text{O-CO}_2$  were calculated  
156 according to the method of Thoning et al. (1989) with a cut-off frequency of 667 days (0.5472 cycles yr<sup>-1</sup>) for a Fast Fourier  
157 Transform (FFT) filter. We also obtained the DMI and ENSO Index from the NOAA/ESRL website (NOAA/ESRL, 2021a;  
158 2021b).



## 159 2.5 Weather data

160 Monthly precipitation data for Nainital uses the monthly precipitation of the state of Uttarakhand, which includes  
 161 Nainital. The data during January 2007 to December 2017 were taken from the rainfall report on the IMD (India Meteorological  
 162 Department) website ([http://hydro.imd.gov.in/hydrometweb/\(S\(fqu5hsvtq3sitn45rjia4qma\)\)/landing.aspx](http://hydro.imd.gov.in/hydrometweb/(S(fqu5hsvtq3sitn45rjia4qma))/landing.aspx)). Monthly  
 163 precipitation data for Comilla uses the average monthly precipitation of Eastern Indo-Gangetic Plain in Bangladesh (Rangpur  
 164 (25.73°N, 89.23°E and 33 m a.s.l.), Sylhet (24.90°N, 91.88°E and 34 m a.s.l.), Bogra (24.84°N, 89.37°E and 18 m a.s.l.),  
 165 Ishurdi (24.13°N, 89.05°E and 13 m a.s.l.), Jessore (23.18°N, 89.17°E and 6 m a.s.l.), Feni (23.03°N, 91.42°E and 6 m a.s.l.),  
 166 Barisal (22.75°N, 90.37°E and 3 m a.s.l.), Chattoogram (22.27°N, 91.82°E and 4 m a.s.l.), and Cox's Bazar (21.43°N, 91.93°E  
 167 and 2 m a.s.l.)). Data during January 2012 to September 2018 were taken from the JMA (Japan Meteorological Agency)  
 168 website (<http://www.data.jma.go.jp/gmd/cpd/monitor/climatview/frame.php?y=2019&m=7&d=30&e=0>).

## 169 2.6 Back trajectory analysis

170 To determine the sources of regional air masses affecting the stations (NTL and CLA), we calculated backward air  
 171 trajectories using the Meteorological Data Explorer (METEX) system (Zeng and Fujinuma, 2004) available via the website of  
 172 the Center for Global Environmental Research, National Institute for Environmental Studies  
 173 (<http://db.cger.nies.go.jp/metex/index.html>). METEX uses three dimensional wind speed (horizontal and vertical wind )  
 174 estimated from the European Centre for Medium Range Weather Forecast (ECMWF) analyses on a  $0.5^\circ \times 0.5^\circ$  mesh to  
 175 calculate 72-h trajectories. We use 1940m for NTL and 30m for CLA as the starting height.

176 The ratio of air mass from south was calculated by the frequency of the air mass from south side on the flask sampling  
 177 date with reference to the backward air trajectories data.

## 178 2.7 Data analysis method for short-term and long-term

179 Mean values for every 10 days were calculated from the weekly data and were used to calculate the long-term trend  
 180 and smoothing fitting curve. The value of the missing period was supplemented with an approximate expression of the values  
 181 before and after the missing period for calculating the continuous long-term trend and smoothing fitting curve.

182 Long-term trends of the mole fractions were calculated based on the idea of Thoning et al. (1989) with a cut-off  
 183 frequency of 667 days ( $0.5472 \text{ cycles yr}^{-1}$ ) for a FFT filter. The smoothing fitting curve was made for an FFT filter with a cut-  
 184 off frequency of 50 days ( $7.3 \text{ cycles yr}^{-1}$ ).

185 We defined and expressed seasonal component by a “ $\Delta$ ” term (e.g.,  $\Delta\text{CO}_2$ ) which was calculated by subtraction of the  
 186 long-term trend curve from 10 days mean of real data. Also, we defined and expressed short-term variations by a “d” term  
 187 (e.g.,  $d\text{CO}_2$ ), which were characterized by the deviation of 10 days mean of real data from the smoothing fitting curve. Figure  
 188 2(c) shows how such components were calculated. Growth rates of mole fraction of observed gases were calculated using the  
 189 long-term trends.

## 190 3. Results and discussion

### 191 3.1 Overview of GHGs levels at both sites

192 Basically, the air masses over the Indian subcontinent were transported from the Indian Ocean region during summer  
 193 (monsoon season) and from the inland during winter. Air mass trajectories are shown for our sampling sites and related sites  
 194 in Figure 3. In the case of anthropogenic GHGs, except  $\text{CO}_2$ , their mole fractions at CLA generally showed relatively low  
 195 levels when the air mass came from the ocean, while the mole fractions were relatively high when the air mass came from  
 196 inland. On the other hand, mole fractions of GHGs at NTL overall did not show relatively low levels, even if the air mass came  
 197 from the Indian Ocean region (i.e., south-eastern wind) because the air mass from Indian Ocean was strongly affected by local



GHGs emissions while passing over the Indo-Gangetic Plain. However, the CO<sub>2</sub> mole fraction changed not only due to transport but also due to the photosynthetic sink strength of terrestrial ecosystems and cultivated crops.

Annual mean GHG mole fractions at NTL and CLA are summarized in Table 1. Annual CO<sub>2</sub> mole fractions at both sites were quite low compared to MLO and other Indian sites such as CRI. For example, in 2010, 386.5 ppm was reported at NTL, 391.9 ppm at CRI (Bhattacharya et al., 2009), and 391.3 ppm was reported at PON (Lin et al. 2015). Note that there is no data for CLA in 2010, however the annual CO<sub>2</sub> mole fraction at CLA is usually only 1–2 ppm higher than at NTL. This seemed to be due to the influence of photosynthesis at both sites. Generally, the CO<sub>2</sub> mole fractions at NTL and CLA decreased strongly (typically twice a year) due to photosynthesis of local crops, making the annual CO<sub>2</sub> levels lower than at other sites despite the likelihood that anthropogenic emission are high in this area.

On the other hand, the annual mean mole fractions of CH<sub>4</sub>, CO, H<sub>2</sub>, and N<sub>2</sub>O at NTL and CLA (Table 1) were almost at the highest levels on the Indian subcontinent due to the influence of strong emission sources. For example, the annual mole fractions of NTL and CLA were 50–470 ppb, 30–200 ppb for CO, and 0–5 ppb for N<sub>2</sub>O higher compared to other Indian sites (e.g., CRI [Bhattacharya et al., 2009], HLE, PON, and PBL [Lin et al., 2015]). In this region, high CH<sub>4</sub> and N<sub>2</sub>O emissions were possible from paddy fields and cultivated areas. Also, much CO is considered to be produced by biomass burning in this region. As for H<sub>2</sub>, the mole fraction at CLA was higher than those at other Indian sites, however, it was relatively low at NTL compared to other sites such as CRI (Bhattacharya et al., 2009), PON, and PBL (Lin et al., 2015), but similar to HLE, which is located on a higher mountain. In the case of the SF<sub>6</sub> mole fraction, it has smaller regional differences, suggesting there are no remarkable SF<sub>6</sub> sources near the measurement sites. Below we describe in detail the characteristics of sources and sinks of each component (CO<sub>2</sub>, δ<sup>13</sup>C-CO<sub>2</sub>, δ<sup>18</sup>O-CO<sub>2</sub>, CH<sub>4</sub>, CO, H<sub>2</sub>, N<sub>2</sub>O, and SF<sub>6</sub>) at NTL and CLA on the Indo-Gangetic Plain in terms of seasonal variations, amplitudes, and growth rates.

### 3.2 CO<sub>2</sub> and δ<sup>13</sup>C-CO<sub>2</sub>

#### 3.2.1 CO<sub>2</sub> mole fraction and growth rate variations

Figure 4 shows the time series of the atmospheric CO<sub>2</sub> mole fraction and the isotopic ratio of δ<sup>13</sup>C-CO<sub>2</sub> at our sampling sites (NTL and CLA) together with data from CRI on the west coast of India and MLO in Hawaii. The CO<sub>2</sub> mole fractions at NTL and CLA in August–October were characteristically lower (approximate 10–20 ppm) than the mole fractions observed at CRI and MLO. The CRI and MLO sites are representative of CO<sub>2</sub> mole fractions in the Southern and Northern Hemisphere, respectively, for the period of the southwest monsoon season (June–September). On the other hand, the δ<sup>13</sup>C-CO<sub>2</sub> at NTL and CLA were inversely correlated with the CO<sub>2</sub> mole fractions, and generally the values at both sites were higher than at MLO and CRI.

Air masses at NTL and CLA in August–October passed over the Indo-Gangetic Plain and the southeast area of India, respectively, while the air masses of CRI were transported from the Indian Ocean region (Fig. 3). Thus, it was suggested that the air mass from the Indian Ocean in August–October prevailing over CRI was hardly influenced by anthropogenic emission and photosynthesis over the Indian subcontinent, whereas CO<sub>2</sub> mole fractions over NTL and CLA seemed to be influenced during these season by the sources and sinks on the Indo-Gangetic Plain and the south/east areas of the Indian subcontinent. Such transport characteristics must affect the annual average and growth rates in the CO<sub>2</sub> molar ratio and δ<sup>13</sup>C-CO<sub>2</sub> in addition to their seasonal variations.

We show the CO<sub>2</sub> growth rates observed at NTL, CLA, and MLO in Figure 5(a). Mean CO<sub>2</sub> growth rate at NTL (approximately 2.0 ppm yr<sup>-1</sup> during 2007–2020) and CLA (approximately 3.1 ppm yr<sup>-1</sup> during 2013–2020) were similar to other sites (e.g., MLO). However, variations of the calculated growth rates were greater than those at MLO. The range was 0–5 ppm yr<sup>-1</sup> in the case of NTL, and CLA had higher variability than NTL because local sink and source influences affected the concentration more than remote sites such as MLO. In general, Pacific sites such as MLO and Japanese remote sites in the Northern Hemisphere showed a relationship between CO<sub>2</sub> growth rates and the ENSO index (e.g., Keeling, 1998). This





relationship is often explained from the viewpoint of a global temperature anomaly, which has a strong relationship with the ENSO index. On the other hand, the variability at NTL has no associations with the variability in the CO<sub>2</sub> growth rate at MLO and the ENSO index (Fig. 5[b]). Both growth rates seemed to be slightly inversely correlated with each other from 2007 to 2015. However, since then, similar relatively high growth rates have been observed for both sites around 2015–2016 and 2018–2019, indicating that overall, the CO<sub>2</sub> growth rate at NTL is less correlated with the CO<sub>2</sub> growth rate at MLO and the ENSO index.

It is well known that the Indian Ocean Dipole controls meteorological conditions such as air mass transportation and precipitation patterns on the Indian subcontinent (e.g., Saji et al., 1999, Ashok et al., 2004, Hong et al., 2008). Such changes in regional climatic pattern could affect the CO<sub>2</sub> uptake flux by plants in the surrounding area and the atmospheric movement, leading to a change in the CO<sub>2</sub> growth rate. However, we did not find a simple relationship between DMI and CO<sub>2</sub> growth rate at NTL (Fig. 5[b]). Here we have shown that the pattern of CO<sub>2</sub> growth rate in this region is different from the global pattern seen in places like MLO, but the relationship between local climatic factors and changes in CO<sub>2</sub> sinks and emissions is likely to be complex, and further study is needed to interpret the differences.

### 3.2.2 Seasonal variation and its characteristics

Figure 6(a)–(d) show the seasonal variations in CO<sub>2</sub> mole fractions and isotopic ratios of  $\delta^{13}\text{C-CO}_2$  at NTL, CLA, CRI, and MLO, which were calculated by subtraction of the measured value from the long-term trend. The annual amplitudes of the CO<sub>2</sub> mole fraction (Table 2) at NTL ( $22.1 \pm 3.9$  ppm) and CLA ( $20.3 \pm 5.7$  ppm) were much larger than those at other Indian sites (CRI, 15 ppm; HLE, 8.2 ppm; PON, 7.6 ppm; PBL, 11.1 ppm). Also, the annual amplitudes of  $\delta^{13}\text{C-CO}_2$  at NTL ( $0.96 \pm 0.16\text{‰}$ ) and CLA ( $0.85 \pm 0.19\text{‰}$ ) were larger than that at CRI (approximately 0.6‰). These results suggested that the atmospheric CO<sub>2</sub> mole fraction of NTL and CLA were strongly influenced by photosynthesis of local plants in summer and their respiration in winter, and other anthropogenic emission which were moderated at the other sites by the influence of the oceanic air.

As shown in Figure 4 (a) and (b) and Figure 6(b) and (d), the seasonal variation pattern at CLA has two lower seasons in CO<sub>2</sub> and two higher seasons in  $\delta^{13}\text{C-CO}_2$  in February–April and July–October. Similarly, in the case of NTL, we sometimes observed relatively low mole fractions of CO<sub>2</sub> in February–March and September, and higher  $\delta^{13}\text{C-CO}_2$ . Especially, the CO<sub>2</sub> mole fraction at CLA in February–March decreased remarkably, by up to approximately 8 ppm. In general, in many cases including at MLO, only a summer minimum CO<sub>2</sub> mole fraction is observed, while a minimum in February–March is not usually observed.

Twice-yearly decreases in the CO<sub>2</sub> mole fraction have also been observed at several Indian sites such as Dehradun (northern Indian site; Sharma et al., 2013), Sinhgad (western Ghats site; Tiwari et al., 2014), Ahmedabad (western Indian site; Chandra et al., 2016), Shadnagar (central Indian site; Sreenivas et al., 2016), and PON (southeast coast Indian site; Lin et al., 2015), however, these studies did not clearly mention such variations. Umezawa et al. (2016) reported that the decrease in the CO<sub>2</sub> mole fraction near the ground in February–March was caused by photosynthesis of local crops, which was detected by the vertical CO<sub>2</sub> profiles over New Delhi airport. Those sites are located on the Indo-Gangetic Plain or received air masses passing over the Indo-Gangetic Plain or Indian subcontinent. On the other hand, the decrease in the CO<sub>2</sub> mole fraction in February–March was not detected at CRI (west coast Indian site; Bhattacharya et al., 2009), HLE (northwestern Himalayan site), or PBL (Andaman Island’s site) (Lin et al., 2015). These sites are not located on the Indo-Gangetic Plain. Thus, air masses at these sites must be mainly transported from the ocean or from areas other than the Indian subcontinent during these periods.

The characteristic CO<sub>2</sub> seasonal variation on the Indo-Gangetic Plain (including NTL and CLA) is very likely to be related to CO<sub>2</sub> uptake by regional vegetation. In the region near NTL, rice, wheat, and other cereals and millets were mainly



282 cultivated (DAC/MA, 2015; SID/MP, 2018; and DES/MAFW, 2019). Generally, in the case of Uttar Pradesh state located in  
 283 the center of the Indo-Gangetic Plain, rice and other summer plants (maize, millets, etc.) are planted mainly in June–July and  
 284 harvested in October–November, while large areas of wheat are sown in October–December and harvested in March–April.  
 285 Therefore, relatively low CO<sub>2</sub> mole fractions observed in those periods are considered to be due to CO<sub>2</sub> uptake by plants  
 286 cultivated in each season near NTL. Panigrahy et al. (2010) reported the main rice growing seasons in North India to be July–  
 287 September and February–March by using the Normalized Difference Vegetation Index (NDVI). Nayak et al. (2010) also  
 288 reported that Net Primary Productivity (NPP) on the Indo-Gangetic Plain increased in August–September and February–March,  
 289 estimated from the NDVI.

290 In Bangladesh, rice, being the staple food, is cultivated three times a year in some regions. Usually rice is grown twice  
 291 (*Aus* and *Amon* rice) from April–October (including the monsoon season), however, often rice is also cultivated (*Boro* rice) in  
 292 the winter season from November–April (SID/MP, 2018). Other agricultural products include maize, jute, and vegetables in  
 293 the summer season, and small amount of wheat in the winter season. Therefore, we concluded that the observed lower CO<sub>2</sub>  
 294 mole fractions in July–October and February–March were influenced by CO<sub>2</sub> uptake by local plants (mainly rice). Especially  
 295 at CLA, the lower mole fraction in February–March was clear and a strong contribution from CO<sub>2</sub> uptake from *Boro* rice was  
 296 estimated. As another viewpoint on CO<sub>2</sub> seasonal variation, we observed that the CO<sub>2</sub> maximum in May was not so high, while  
 297 the CO<sub>2</sub> mole fraction in December was higher. Because precipitation in Bangladesh is stronger than in the north Indian region,  
 298 the duration of rice cultivation over summertime is also longer than in north India. Therefore, the contribution of plant uptake  
 299 to the CO<sub>2</sub> mole fraction in the atmosphere at CLA over the summer season is likely to be relatively large compared to that at  
 300 NTL.

301 Thus, the decreases in the CO<sub>2</sub> mole fractions in February–March and September in NTL and CLA were estimated to  
 302 be caused by photosynthesis of plants cultivated in each season over the Indo-Gangetic Plain. NTL and CLA indicated this  
 303 more clearly compared with other Indian sites due to the proximity to the source region. Figure 7(a) shows the relationships  
 304 between the annual mean CO<sub>2</sub> mole fraction and  $\delta^{13}\text{C-CO}_2$  in 2010 and 2012. The slope between the CO<sub>2</sub> mole fraction and  
 305  $\delta^{13}\text{C-CO}_2$  showed  $-0.050$  and  $-0.054\text{‰ ppm}^{-1}$  which indicated that the spatial variability of the atmospheric CO<sub>2</sub> mole fraction  
 306 (e.g., a lower mole fraction at NTL than at MLO and CRI) basically occurred due to CO<sub>2</sub> exchange between the atmosphere  
 307 and terrestrial biosphere.

308 Furthermore, we examined the relationship of the CO<sub>2</sub> mole fraction and carbon isotope ratio, because there are some  
 309 seasonal differences in the species cultivation. On the Indo-Gangetic Plain, rice (especially in Bangladesh) and wheat  
 310 (especially in North India), as C<sub>3</sub> plants, are cultivated in January–March, while C<sub>4</sub> plants (e.g., maize, sugarcane, sorghum  
 311 and Bajra (Pearl millet) in addition to rice are cultivated on the Indo-Gangetic Plain and in Bangladesh in June–September  
 312 (DAC/MA, 2015; SID/MP, 2018; DES/MAFW, 2019). We calculated the end member of the isotope value for absorbed CO<sub>2</sub>  
 313 by using intercept values of the “Keeling plot” between the reciprocal of the CO<sub>2</sub> mole fraction and the ratio of  $\delta^{13}\text{C-CO}_2$   
 314 obtained from two continuous datasets of air samples, which has  $> 1$  ppm difference in CO<sub>2</sub> mole fraction and  $> 0.05\text{‰}$  in  
 315  $\delta^{13}\text{C-CO}_2$ . Since in this study two datasets had 1-week intervals, we assumed that the difference in CO<sub>2</sub> and  $\delta^{13}\text{C}$  between two  
 316 datasets would include broader influences of photosynthetic activities from relatively large areas on the Indo-Gangetic Plain.

317 We found that the intercept values of NTL and CLA showed differences in January–March and June–September (Fig.  
 318 7[b]), which appeared to reflect the differences in the contributions of C<sub>3</sub> and C<sub>4</sub> plants in this region. In June–September, we  
 319 found relatively heavier intercept values at both NTL ( $-25.0 \pm 2.4\text{‰}$ ) and CLA ( $-23.5 \pm 4.1\text{‰}$ ), suggesting that C<sub>4</sub> plants partly  
 320 contributed to the CO<sub>2</sub> absorption (or emission) in this season, while in January–March, the end member showed  $-29.0 \pm 4.3\text{‰}$   
 321 (NTL) and  $-28.3 \pm 4.0\text{‰}$  (CLA), which were similar to the general C<sub>3</sub> plant (rice or wheat). If we assume the value for C<sub>4</sub> plant  
 322 to be  $-12$  to  $-14\text{‰}$ , the contributions of C<sub>4</sub> plant in NTL and CLA were approximately  $25 \pm 5\%$  and  $31 \pm 9\%$ , respectively.  
 323 According to database (DAC/MA, 2015; SID/MP, 2018; DES/MAFW, 2019) for crops area in Uttar Pradesh district, the area’s  
 324 ratio of C<sub>4</sub> plants (e.g., maize and sugarcane) to C<sub>3</sub> plants in the summer season was approximately 26% in 2012, which was





a similar proportion as estimated by the C isotope ratio. In the case of Bangladesh, despite there being no recent data reported, according to data in 2008, the area for maize was approximately < 10% compared to the rice area. However, based on the recent C isotope ratio, it appears likely that more maize has been cultivated.

### 3.3 $\delta^{18}\text{O}\text{-CO}_2$

In general,  $\delta^{18}\text{O}\text{-CO}_2$  is related to that value of water in plants and soil, because oxygen atom of  $\text{CO}_2$  can be exchanged with oxygen atom of  $\text{H}_2\text{O}$  in plant and bacteria cells during photosynthesis and soil respiration. Plants and soil water mainly originate from rainwater in the study region, however, in the case of the agricultural area, water is often introduced by irrigation systems using river and groundwater. In many cases, photosynthesis produced relatively heavier  $\delta^{18}\text{O}\text{-CO}_2$  than soil respiration because  $\delta^{18}\text{O}\text{-H}_2\text{O}$  in plant becomes heavier than soil water due to plant transpiration.

Larger amplitudes (approximately 3‰) in the seasonal variation of  $\delta^{18}\text{O}\text{-CO}_2$  at both NTL and CLA were observed, compared to that of MLO (approximately 0.4‰) (Fig. 8[a]). The isotopic ratio of  $\delta^{18}\text{O}\text{-CO}_2$  at CRI (Bhattacharya et al., 2009) was reported to have similar seasonal variation (i.e., high in winter [November–February] and low in September) to our sites. In the Pacific sites like MLO,  $\delta^{18}\text{O}\text{-CO}_2$  has a maximum peak from spring to summer when photosynthesis activity become dominant, while a minimum is seen around fall when the contribution of soil respiration exceeds that of photosynthesis. On the other hand, Indian subcontinent sites seemed to have fairly different seasonal variation patterns, having a maximum in January–February, gradually decreasing from March–September/October, and subsequently rapidly increasing (Fig. 8[c] and [d]). Such seasonal variation may be influenced by photosynthesis and soil respiration in these regions. However, because many crops are cultivated through the year in these areas (as mentioned in section 3.2), the contribution of photosynthesis to the seasonal variation may be relatively small. High soil respiration activity in the wet season can contribute a little more than during the dry season.

On the other hand, seasonal variations in  $\delta^{18}\text{O}$  of rainwater itself seemed to affect  $\delta^{18}\text{O}\text{-CO}_2$  through photosynthesis and respiration processes. For example, Sengupta and Sarkar (2006) showed the  $\delta^{18}\text{O}\text{-H}_2\text{O}$  in rain at New Delhi (western Indo-Gangetic Plain) had a higher value in March–May and a minimum value in September. Such variation was fairly consistent with the seasonal variation in  $\delta^{18}\text{O}$  of  $\text{CO}_2$  at NTL. Similarly, CLA has a minimum  $\delta^{18}\text{O}\text{-CO}_2$  in the atmosphere in October, which was the same month in which the minimum  $\delta^{18}\text{O}\text{-H}_2\text{O}$  was observed in rain in Eastern Indo-Gangetic Plain areas (e.g., Kolkata [near Bangladesh; Sengupta and Sarkar, 2006] and Cherrapunji [Eastern Indo-Gangetic Plain; Breitenbach et al., 2010]). During the rainy season, due to the so-called “amount effect”,  $\delta^{18}\text{O}\text{-H}_2\text{O}$  in rain will decrease with an increase in the amount of precipitation (e.g., Rozanski et al., 1993). However, in the Indian region it has been reported that seasonal changes in the origin of moisture strongly affected the  $\delta^{18}\text{O}\text{-H}_2\text{O}$  (Sengupta and Sarkar, 2006, Tanoue et al., 2018). In winter (i.e., when there is less rain), moisture comes from the west or north. Therefore, the northern area of the Arabian Sea and the western land area supply moisture, which has a higher  $\delta^{18}\text{O}\text{-H}_2\text{O}$ . However, the air mass in the summer monsoon season (mainly June–September) comes from the southern part of the Arabian Sea and sometimes passes over the Bay of Bengal carrying much moisture. The value of  $\delta^{18}\text{O}\text{-H}_2\text{O}$  in the moisture in the air mass decreases with the process of raining along the air trajectory. In the post-monsoon season (mainly October–December), some portion of moisture comes from the Pacific, Bay of Bengal, and the inland area (Tanoue et al., 2018).

In the winter monsoon season (mainly February–May),  $\delta^{18}\text{O}\text{-H}_2\text{O}$  in rain was reported to be approximately 0–1‰ (vs VSMOW). During the winter monsoon season, there is little precipitation, so plant cultivation utilizes irrigation systems using river and groundwater. River and groundwater usually show not so large seasonal variation in  $\delta^{18}\text{O}$  and have a close value to the annual mean of  $\delta^{18}\text{O}\text{-H}_2\text{O}$  in rain, such as -6 to -8‰ (Kumar et al., 2019). According to the variation of  $\delta^{18}\text{O}\text{-CO}_2$ , in winter its value was approximately 2‰ (vs VPDB- $\text{CO}_2$ ; VPDB- $\text{CO}_2$  scale is fairly close to the scale of  $\text{CO}_2$  equilibrated with VSMOW water as mentioned in section 2.3), which was higher than that of rain and other water reservoirs, suggesting that  $\delta^{18}\text{O}\text{-H}_2\text{O}$  in plants and soil must become higher due to transpiration during dry and relatively warm conditions in winter.



Based on the fact that during the summer monsoon season,  $\delta^{18}\text{O}\text{-CO}_2$  decreased from 1 to -2‰ with a decrease of  $\delta^{18}\text{O}\text{-H}_2\text{O}$  from 0 to -10 or -15‰ in the rain, the range of variation in  $\delta^{18}\text{O}\text{-CO}_2$  was approximately one third or one fifth that of rain. Because land water may come from both rain and irrigation systems, the real ranges of  $\delta^{18}\text{O}$  in soil water and plant water are likely to be smaller than in the case of rain only. Furthermore, because  $\text{CO}_2$  from soil respiration contributes more in the rainy season, a balance between photosynthesis and respiration  $\text{CO}_2$  will, in general, have a small effect on the seasonal variation.

As for the annual trend of  $\delta^{18}\text{O}\text{-CO}_2$  shown in Figure 8(b), NTL showed a similar pattern to that of MLO whereas CLA showed a different trend. The  $\delta^{18}\text{O}\text{-CO}_2$  at NTL began at 0.8‰ in 2007, decreased to 0.2‰ in 2011, then again became heavier (toward 1.0‰) during 2014–2016 (Fig. 8[b]). In northern India, relatively high precipitation was reported during 2011–2013. The tendency of lower  $^{18}\text{O}\text{-CO}_2$  may have some relationship with the amount of precipitation. In 2008 and 2016 considerable amounts of precipitation fell near NTL. The  $^{18}\text{O}\text{-CO}_2$  level also seemed to become relatively low. A La Nina event occurred from late 2010 to 2012 and the amount of precipitation increased worldwide from 2010 to 2013. Such large-scale climatic effects are very likely to affect the  $^{18}\text{O}\text{-CO}_2$  level observed at MLO. In the case of CLA, precipitation increased in 2015–2017 (rather than in 2011–2013) and the  $^{18}\text{O}\text{-CO}_2$  level at CLA seemed to become lower at that time with the increase of precipitation. Analyzing the relationship between the monthly amount of precipitation and  $\delta^{18}\text{O}\text{-CO}_2$  in Figure 8(e) and (f), a weak negative correlation can be seen. Therefore, the amount of precipitation partly contributes to the regional level of  $\delta^{18}\text{O}\text{-CO}_2$ . However, it must be influenced not only by precipitation but also by seasonal changes in air flow patterns and rain systems, as explained above, as well as by the water reservoir situation, soil water content at that time, and photosynthesis in the region.

If the ground water storage decreases due to wider usage of irrigation and/or less precipitation in recent times, it causes a stronger transpiration effect in the soil environment, making the  $\delta^{18}\text{O}$  of soil water heavier than usual. Roxy et al. (2015) and Asoka et al. (2017) reported that precipitation over the Indian subcontinent and groundwater storage in northern India has had a decreasing trend due to Indian Ocean warming, which is estimated to have occurred due to the weakening trend of the summer monsoon cross-equatorial flow (Swapna et al., 2014). However, much longer records of  $\text{CO}_2$  isotopic ratios are needed to clarify the increasing trend in  $\delta^{18}\text{O}\text{-CO}_2$  and the relationship with climatic changes in this region.

### 3.4 $\text{CH}_4$

The  $\text{CH}_4$  mole fractions at NTL and CLA are illustrated in Figure 9(a). We detected high  $\text{CH}_4$  mole fractions at NTL and CLA, where they sometimes exceeded 2,100 and 4,000 ppb, respectively, showing that the Indo-Gangetic Plain region had relatively strong  $\text{CH}_4$  emissions. The seasonal amplitude of the  $\text{CH}_4$  mole fraction, especially at CLA ( $486 \pm 225$  ppb; Table 2) was much larger than the those of other Indian sites such as NTL (114 ppb), CRI (200 ppb) (Bhattacharya et al., 2009), Darjeeling (400 ppb) (Ganesan et al., 2013), HLE (29 ppb), PON (124 ppb), and PBL (144 ppb) (Lin et al., 2015), which indicated that the contribution of the  $\text{CH}_4$  source (e.g., rice cultivation) around CLA was relative strong.

Mean seasonal variations in the  $\text{CH}_4$  mole fraction for both sites were calculated and are shown in Figure 9(c) and (d). The mole fractions at both NTL and CLA had the highest peak in August–October and a small peak in March. In general, the  $\text{CH}_4$  mole fraction in the Northern Hemisphere decreased in July–September (summer season) through the decomposition process by reaction with OH radicals during this period. A higher  $\text{CH}_4$  mole fraction in this period strongly suggests that there are some sources of  $\text{CH}_4$ . Observation results at Darjeeling (north-eastern Indian site; Ganesan et al., 2013), HLE (Lin et al., 2015), and Shadnagar (Sreenivas et al., 2016) also indicated high  $\text{CH}_4$  mole fractions during August–October. Ganesan et al. (2013) reported that the  $\text{CH}_4$  mole fraction at Darjeeling was enhanced by transported air masses from the Indo-Gangetic Plain. Lin et al. (2015) and Sreenivas et al. (2016) showed that the high  $\text{CH}_4$  mole fractions at HLE and Shadnagar were influenced by emissions from paddy fields and wetlands. Garg et al. (2011) showed that  $\text{CH}_4$  emission from rice fields was estimated to be approximately 17% of the total  $\text{CH}_4$  emissions in India. According to the emission database of EDGAR v4.3.2 (EC-JRC/PBL, 2016), rice cultivation was the largest source of  $\text{CH}_4$  (approximately 50%) in Bangladesh.



Bhatia et al. (2011) measured the CH<sub>4</sub> flux from paddy fields at New Delhi and showed that it was the highest in August–September due to the increase in the activity of rice roots and bacteria in the paddy field soils. Ali et al. (2012) also measured the CH<sub>4</sub> flux from paddy fields at Bangladesh and reported that the CH<sub>4</sub> flux was maximized within 77–98 days after the planting of rice due to the increase in root respiration and carbon in soil. It was considered that both March and September–October were consistent with the timing of increasing CH<sub>4</sub> production at rice fields according to the customary cultivation schedule of rice in this region. In Bangladesh and the eastern Indian district, rice is cultivated from November–September, as mentioned above in the CO<sub>2</sub> section, and CH<sub>4</sub> emissions are considered to continue during winter, supporting higher CH<sub>4</sub> mole fractions from August–March, especially at CLA.

On the other hand, CRI (Bhattacharya et al., 2009), PON, and PBL (Lin et al., 2015) did not show higher CH<sub>4</sub> mole fractions in August–October, as shown in Figure 9(c) and (d). The air masses at those sites in August–October were transported from the Indian Ocean, which may have only a minimal influence from agricultural emission.

CH<sub>4</sub> mole fractions at NTL and CLA were higher than that at MLO, even at the time of year when rice is not cultivated. CH<sub>4</sub> emissions from the enteric fermentation and wastewater handling were reported to be large sources according to the emission database in EDGAR v4.3.2 (EC-JRC/PBL, 2016). Garg et al. (2011) reported that enteric fermentation by cattle and buffalo contributes approximately 40% emissions in India. Such CH<sub>4</sub> emissions must always elevate the CH<sub>4</sub> mole fraction in the air mass in these sites regardless of the season.

In addition, biomass burning (including residential cooking and agricultural residue burning) is very likely to have contribution to the CH<sub>4</sub> mole fraction according to the inventory evaluation (i.e., 21% contribution; Garg et al, 2011). Reasonably good correlations were seen between short term components in variations of CH<sub>4</sub> and CO in January–March, April–June, and October–December. Ratios of dCH<sub>4</sub> to dCO showed ranges such as 0.64–0.80 ppb ppb<sup>-1</sup> in NTL and 1.85–1.98 ppb ppb<sup>-1</sup> in CLA, as shown in Figure. 9(e) and (f). One of the major CO sources in India was considered to be biomass burning (Dickerson et al., 2002). Akagi et al (2011), EC-JRC/PBL (2016), and Sfez et al. (2017) reported that the emission ratios of CH<sub>4</sub> to CO in biomass burning such as crop residue burning, firewood burning, and biogas burning were 0.04–0.90 ppb ppb<sup>-1</sup>. Therefore, the ratios observed in these seasons could suggest a strong influence on CH<sub>4</sub> and CO emissions from biomass burning (such as crop residue burning), despite the other large CH<sub>4</sub> emissions such as paddy fields and waste treatment, which will increase the ratio, especially at CLA in July–September.

As a result, it is evident that annual CH<sub>4</sub> mole fractions at the sites used in this study on the Indo-Gangetic Plain are enriched by various CH<sub>4</sub> sources, depending on the season. Generally speaking, because April–June is a dry and hot season, CH<sub>4</sub> decomposition processes will proceed, decreasing its mole fraction at both sites.

The variability in the CH<sub>4</sub> growth rate in the trend line at NTL was different to the variability at MLO (Fig. 9[b]), which may be influenced by regional climatic condition, including the Indian Ocean Dipole. Because the frequency of air mass transportation from the south increased if the Indian Ocean Dipole was often activated, the air mass passed over the Indo-Gangetic Plain (which has strong CH<sub>4</sub> emissions), reaching NTL with a high CH<sub>4</sub> mole fraction. The difference between the variability in the CH<sub>4</sub> growth rate between NTL and CLA may also be explained by the above hypothesis. If the frequency of air mass transportation from the south increased by the activation of Indian Ocean Dipole (e.g., in 2015) because the air mass was directly transported from the Indian Ocean with a relatively low CH<sub>4</sub> mole fraction, the CH<sub>4</sub> mole fraction at CLA would become relatively low compared to a usual year (Fig. 9[b]). On the other hand, as mentioned previously, in 2015–2017, even in high Indian Ocean Dipole mode, Bangladesh had relatively high precipitation which could strengthen CH<sub>4</sub> production from rice paddy fields and other aquatic environments. This potential situation well-matched the high CH<sub>4</sub> mole fraction in summer and the high growth rate at CLA during 2016–2017.



### 448 3.5 CO

449 High annual CO mole fractions at both NTL and CLA (Table 1) indicated that the atmosphere over the Indo-Gangetic  
450 Plain was influenced by strong CO emission sources such as burning of harvest residues and residential burning using solid  
451 biofuel, which are considered to be main CO emission sources in the region (EC-JRC/PBL, 2016). However, of course, CO  
452 originating from car exhaust and industrial activities remains very likely to have made some contributions to the CO mole  
453 fraction (EC-JRC/PBL, 2016).

454 The main crops around NTL are rice and wheat and the harvesting periods are September–November and April–May,  
455 respectively (DAC/MA, 2015). Farmers in this area generally burn harvest residues at their farmland after harvest (Lohan et  
456 al., 2018). Venkataraman et al. (2006) reported that the amount of burning on the Western Indo-Gangetic Plain has two peaks  
457 annually, i.e., in May and November. We could observe the same seasonal variation (i.e., two mole fraction peaks in May and  
458 November) in the CO mole fraction in the atmosphere at NTL (Fig. 10[c]). Sharma et al. (2010) suggested that the high CO  
459 mole fraction on the Western Indo-Gangetic Plain is emitted in October by the burning of harvest residues, based on data from  
460 satellite observations. Kumar et al. (2011) also reported that the highest densities in fire spots were seen in spring and autumn  
461 on the western Indo-Gangetic Plain. These suggested that CO emissions from the burning of harvest residues was one of the  
462 most important sources on the Western Indo-Gangetic Plain in these seasons.

463 On the other hand, the seasonal variation in CO mole fraction at CLA exhibited only one peak in October–March (Fig.  
464 10[d]). Such seasonal variation was also detected at CRI (Bhattacharya et al., 2009), PON, PBL (Lin et al., 2015), and  
465 Ahmedabad (Chandra et al., 2016). In Bangladesh, after the end of the monsoon (October–March), harvest residues are burnt  
466 and used to make bricks using some kinds of biofuel as a heat source (Guttikunda et al., 2012). Also, dung is burnt for the  
467 stove (Venkataraman et al., 2010) during the winter season. In addition, biofuel is used for cooking (Lawrence and Lelieveld,  
468 2010) throughout the year. Those activities could emit large amounts of CO (Streets et al., 2003; Venkataraman et al., 2010;  
469 Maithel et al., 2012).

470 In addition, the seasonal amplitude of the CO mole fraction (Table 2) at CLA ( $356 \pm 90$  ppb) on the Eastern Indo-  
471 Gangetic Plain site was much larger than that observed in other Indian sites (e.g., CRI [200 ppb], PON [78 ppb], PBL [144  
472 ppb], and Ahmedabad [270 ppb]). The highest CO amplitude observed at CLA was consistent with the model estimation of  
473 CO emissions, which showed that the Eastern Indo-Gangetic Plain included areas with the highest CO emissions (Kumar et  
474 al., 2013).

475 On the other hand, the annual mean CO mole fraction at NTL gradually decreased approximately by 50 ppb for 10  
476 years (2006–2015; Fig. 10[a]). Especially, the monthly mean CO mole fraction in November of each year (i.e., the highest  
477 level in the year) at NTL decreased by 120 ppb during that period. This suggests that the amount of harvest residues burnt  
478 decreased, the ratio of incomplete combustion in car engines was improved, or the type of fossil fuel for cooking changed from  
479 biofuel to natural gas. Such decreasing trends in the CO mole fraction level were also detected by Pandey et al. (2017) who  
480 reported total-column CO levels during 2003–2014 over the Indo-Gangetic Plain. However, the CO mole fraction level at NTL  
481 appeared to increase slightly from 2015. Although the reason for the increase is unclear from this study only, CO emissions  
482 from car exhaust were recently estimated to have increased (EC-JRC/PBL, 2016). Therefore, further monitoring is important.

483 The trend in the CO mole fraction and its inter-annual variability at NTL was similar to those in CH<sub>4</sub> at NTL (Fig. 9[b]  
484 and Fig. 10[b]). The mole fractions of CO and CH<sub>4</sub> at NTL tended to be slightly higher when the air mass passed over the  
485 Indo-Gangetic Plain, where there are strong sources of both CO and CH<sub>4</sub>. In 2015 and 2017, a large positive Indian Dipole  
486 Mode occurred, in addition to El Niño in 2015. Therefore, we observed more frequent southern winds, causing higher CH<sub>4</sub>  
487 and CO mole fractions at NTL. However, at CLA, southern wind will decrease the mole fraction of CO. Thus, temporal  
488 variations of both CO and CH<sub>4</sub> mole fractions in both sites must be strongly controlled by meteorological conditions as well  
489 as source strength.



### 490 3.6 H<sub>2</sub>

491 Mole fractions, growth rates, and seasonal variations of H<sub>2</sub> at both sites are shown in Figure 11(a-d). It was found  
492 that CLA, especially, showed a higher mole fraction than the other sites. Novelli et al. (1999) reported that the mainly sources  
493 of H<sub>2</sub> were combustion (fossil fuel combustion and biomass burning) and photochemical sources such as the oxidation of CH<sub>4</sub>  
494 and non-CH<sub>4</sub> hydrocarbons (NMHCs), which account for 90% of the total source. The other 10% is attributed to emissions  
495 from volcanoes, oceans, and nitrogen fixation by legumes. Therefore, we have to assume that there are some emission sources  
496 at CLA.

497 On the other hand, H<sub>2</sub> is removed from the troposphere by reacting with OH and by deposition and oxidation at  
498 surface soil. The amounts of sources and sinks for H<sub>2</sub> in the global budget were estimated to be equal, resulting in a near-  
499 equilibrium state (Novelli et al., 1999). The strengths of H<sub>2</sub> removal in the atmosphere over the Indian subcontinent do not  
500 differ greatly by region according to Yashiro et al. (2011), whereas the strengths of H<sub>2</sub> sources may differ by region (Price et  
501 al., 2007). Lin et al. (2015) reported that H<sub>2</sub> mole fractions at Indian sites were influenced by biomass burning and were 0–40  
502 ppb higher than those at regional background sites (e.g., eastern Kazakhstan and central China). Figure 11(c) and (d) show the  
503 seasonal variations of the H<sub>2</sub> mole fraction at NTL and CLA, which illustrate the maximum in May and the minimum in  
504 December at NTL, and the maximum in November–January and the minimum in June–August at CLA, which were different  
505 from the averaged seasonal variation in the Northern Hemisphere, which showed the maximum in March–April and the  
506 minimum in August–September (Novelli et al., 1999).

507 Because the burning of biomass (such as harvest residuals and dung) appeared to be actively carried out on the Indo-  
508 Gangetic Plain (including at NTL) during April–May and at CLA during November–February, H<sub>2</sub> production must, therefore,  
509 increase during these seasons. Furthermore, since higher CH<sub>4</sub> mole fractions at NTL and CLA were observed during August–  
510 September and September–October due to strong paddy field emissions at those times, H<sub>2</sub> production from CH<sub>4</sub> degradation  
511 can also increase. Figure 11(e) and (f) show short-term variable components (such as dCO and dH<sub>2</sub>, and dCH<sub>4</sub>, and dH<sub>2</sub>) at  
512 both NTL and CLA during those periods, and that they had positive correlations. These figures may suggest some relationship  
513 between H<sub>2</sub> emission with biomass burning, and between photochemical reactions between OH and CH<sub>4</sub>, respectively.  
514 Furthermore, the minimum H<sub>2</sub> in June–August was influenced by a fresh air mass from the Indian Ocean which is only  
515 minimally affected by anthropogenic emission.

516 As mentioned above, the H<sub>2</sub> mole fraction level at CLA was higher than that at NTL. The amplitude of the seasonal  
517 variation of the H<sub>2</sub> mole fraction (Table 2) at CLA showed  $70.4 \pm 42.2$  ppb, which was also larger than the amplitudes at other  
518 Indian sites such as Nainital (50 ppb), CRI (50 ppb) (Bhattacharya et al., 2009), HLE (22 ppb), PON (16 ppb), and PBL (22  
519 ppb) (Lin et al., 2015). These tendencies were consistent with the results of Price et al. (2007), which indicated a larger H<sub>2</sub>  
520 emission area around the Eastern Indo-Gangetic Plain, such as at CLA, than on the Western Indian subcontinent. Thus, our  
521 observation and previous studies both indicated that the Indian subcontinent had relatively strong H<sub>2</sub> sources.

### 522 3.7 N<sub>2</sub>O

523 Garg et al. (2012) reported that the agricultural sector accounted for approximately 75% of the total N<sub>2</sub>O emission in India  
524 in 2005, including around 49% from nitrogen fertilizer use. In particular, they reported that northern India (the Indo-Gangetic  
525 Plain) has the highest N<sub>2</sub>O emission in India because nitrogen fertilizer was applied to extensive paddy fields, was denitrified,  
526 and N<sub>2</sub>O was produced and emitted to the atmosphere. Ganesan et al. (2013) reported that the N<sub>2</sub>O mole fraction at Darjeeling  
527 (north-eastern Indian site) was enhanced due to air mass transportation from the Indo-Gangetic Plain. The annual mean N<sub>2</sub>O  
528 mole fraction at NTL (Table 1) appeared to be almost the same as at Darjeeling sites in North India and was higher than at  
529 another two Indian sites (CRI [Bhattacharya et al., 2009] and HLE [Lin et al., 2015]) and at MLO (Fig. 12[a]).

530 Thompson et al. (2014) estimated that the N<sub>2</sub>O emissions of the Eastern Indo-Gangetic Plain, including CLA, were  
531 higher than those of the Western Indo-Gangetic Plain. This is supported by our observation results that show that the N<sub>2</sub>O



annual mean mole fraction during 2013–2019 at CLA on the Eastern Indo-Gangetic Plain was 1–2 ppb higher than at NTL on the Western Indo-Gangetic Plain (Table 1), and the seasonal amplitude of the  $\text{N}_2\text{O}$  mole fraction (Table 2) at CLA ( $4.25 \pm 1.45$  ppb) was higher than the amplitudes at other Indian sites (NTL, CRI [Bhattacharya et al., 2009], HLE, PON, and PBL [Lin et al., 2015]). Raut et al. (2011) reported the highest  $\text{N}_2\text{O}$  emission rates in the regions of Bangladesh and Sri Lanka due to their high usage of urea as a fertilizer.

However, interestingly, PON and PBL, where oceanic air from the Bay of Bengal affected the sites (Lin et al, 2015) seemed to have relatively higher mole fractions than the sites in this study. As for the seasonal variation in the  $\text{N}_2\text{O}$  mole fraction at NTL, a higher mole fraction was seen in May–September (Fig. 12[c]). Generally, nitrogen fertilizer was frequently applied to paddy fields in May–September in northern India. Gupta et al. (2016) measured the  $\text{N}_2\text{O}$  flux in paddy fields at New Delhi and reported that the flux increased immediately after the application of nitrogen fertilizer to the fields. Therefore, high  $\text{N}_2\text{O}$  levels and increases in the  $\text{N}_2\text{O}$  mole fraction at NTL in May–September were influenced by the enhancement of the  $\text{N}_2\text{O}$  flux due to the denitrification of nitrogen fertilizer in paddy fields.

The  $\text{N}_2\text{O}$  mole fraction at CLA increased in November–February (Fig. 12[d]) and such seasonal variation was almost identical to the seasonal variation in CO at CLA. The seasonal component in the  $\text{N}_2\text{O}$  mole fraction ( $\Delta\text{N}_2\text{O}$  = deviation of  $\text{N}_2\text{O}$  mole fraction from the long-term trend) at CLA showed positive correlations ( $R^2 = 0.81$ – $0.88$ ) with that of the CO mole fraction ( $\Delta\text{CO}$ ) each year (Fig. 11[e]). Also, their ratio ( $\Delta\text{N}_2\text{O}/\Delta\text{CO}$ ) showed  $0.013$ – $0.015$  ppb ppb<sup>-1</sup>, which was same ( $0.015$  ppb ppb<sup>-1</sup>) as the ratio of total  $\text{N}_2\text{O}$  and total CO emissions in Bangladesh from the EDGAR v4.3.2 database (EC-JRC/PBL, 2016). Although such seasonal variation is likely to be partly related to the lower mixing height in the winter season, variations in  $\text{N}_2\text{O}$  emission flux must affect the seasonal variations in the mole fraction. In general, the CO mole fraction was influenced by biomass burning in this season. Because many inventory data showed that biomass burning produced both  $\text{N}_2\text{O}$  and CO,  $\text{N}_2\text{O}$  may be affected partly emitted from biomass burning. However, the emission ratios of  $\text{N}_2\text{O}$  to CO are fairly variable with an approximate range of  $0.0004$ – $0.017$  (Andreae and Merlet, 2001; Sahai et al., 2007, 2011; EDGAR v4.3.2 [EC-JRC/PBL, 2016]). It seemed that this ratio changes with the type of plants that are burnt. According to Sahai et al. (2011), because the ratio was approximately  $0.004$  in the case of rice straw, some portion (e.g.,  $0.004/0.015$ , i.e., approximately 27% at the most) of  $\text{N}_2\text{O}$  in the atmosphere may originate from biomass burning. In addition, since Venkataraman et al. (2010) reported that dung burning is one of major  $\text{N}_2\text{O}$  sources among many kinds of biomass burning in India, its contribution was also possible.

On the other hand, nitrification and denitrification processes of nitrogen fertilizer in rice paddy soil are considered to be major causes of  $\text{N}_2\text{O}$  emissions in this region (EDGAR v4.3.2), however, the emission rate appeared to have seasonal variation. Related to the irrigation system, the  $\text{N}_2\text{O}$  flux was thought to be larger in alternating wet and dry conditions than under continuously flooded conditions (Akiyama et al., 2005; Gaihare et al., 2018; Begum et al., 2019). In the summer monsoon season, many rice paddies fields in Bangladesh must have enough water level because of the ample amount of precipitation. After the summer monsoon (from October), the water level in the paddy field intermittently changed with the situation. Therefore, relatively a higher  $\text{N}_2\text{O}$  emission rate likely occurred during the winter season, when rice (*Boro* rice) was still grown, enhancing the  $\text{N}_2\text{O}$  mole fraction in the winter season. Further observations of high frequency variations of both  $\text{N}_2\text{O}$  and CO mole fractions will contribute towards precisely evaluating the  $\text{N}_2\text{O}$  emission sources at this site.

The  $\text{N}_2\text{O}$  growth rates at NTL and CLA were similar to that of MLO (Fig. 12[b]), however, the variations in the  $\text{N}_2\text{O}$  growth rate at both NTL and CLA were larger than that of MLO during 2016–2020. The variation in the  $\text{N}_2\text{O}$  growth rate showed a similar pattern to the growth rates of CO and  $\text{H}_2$  (Fig. 9[b] and Fig. 10[b]), indicating that the sources of these gases had basically common characteristics.

### 3.8 $\text{SF}_6$

$\text{SF}_6$  is mainly emitted artificially from factories and urban areas (Olivier et al., 2005). Ganesan et al. (2013) reported that the  $\text{SF}_6$  emission at Darjeeling (northeastern Indian site) was considerably weak. Our results also showed that  $\text{SF}_6$  mole





fractions at NTL and CLA were almost the same as the background SF<sub>6</sub> mole fraction (e.g., MLO in Fig. 13[a] and other sites such as HLE, PON, and PBL [Lin et al., 2015]). In addition, the annual amplitudes of the SF<sub>6</sub> mole fraction at Indian sites (HLE, PON, and PBL) were 0.15, 0.24, and 0.48 ppt, respectively, which were almost within the same range (0.15–0.23 ppt) as at NTL and CLA (Table 2). These results suggested that there was no large SF<sub>6</sub> source on the Indo-Gangetic Plain.

Figure 13(c) and (d) show that the seasonal variations of the SF<sub>6</sub> mole fraction at NTL and CLA decreased in summer (NTL: July, CLA: June–August), which was the same variation as those detected at PON and PBL (Lin et al., 2015). In the summer season, air masses from the south via the Indian Ocean prevailed in the NTL and CLA regions, as shown in Figure 2. Generally, the SF<sub>6</sub> mole fraction in the Southern Hemisphere was lower than that in the Northern Hemisphere (Geller et al., 1997). Thus, the seasonal variation in the SF<sub>6</sub> mole fraction was explained by the frequency of air mass transportation from the south.

Figure 13(b) shows the interannual variability of the SF<sub>6</sub> growth rate at NTL, CLA, and MLO and southern air mass contribution at NTL and CLA. The variability in the SF<sub>6</sub> growth rate at NTL was different to the variability at MLO, and in fact we could see an anticorrelation between them. In the case of CLA, an anticorrelation was not so clear because of a relatively shorter data record. The decrease in the growth rate at NTL seemed to have a relationship with the increase in the frequency of southern air mass transportation. This indicated that the growth rate of the SF<sub>6</sub> mole fraction at NTL may be controlled by the regional climatic condition though the transportation process. Because SF<sub>6</sub> had weaker sources in Northern India, the variation in its trend could be explained more clearly by the influence of the air mass movements.

As mentioned above, anticorrelation in the growth rates between MLO and this region was also seen in CO<sub>2</sub> and CH<sub>4</sub>. Therefore, we must take into consideration the influence of the variation in large-scale atmospheric circulation to the GHG mole fraction and trends in their growth rates in the Indian region.

#### 4. Conclusions

We characterized GHGs and related gases over the Northern Indian region using air samples collected weekly at Nainital, India (NTL), and Comilla, Bangladesh (CLA), since 2006 and 2012, respectively. Observation data at both NTL and CLA were compared with the GHG data of other Indian sites and Mauna Loa, Hawaii (MLO) in the Pacific station. From this comprehensive analysis, it was found that the feature of seasonal and long-term variations in each gas were influenced by the local sinks and sources during each season, and annual climatic conditions on the Indo-Gangetic Plain. They were considerably different to those of the MLO in the Pacific region.

On the Indo-Gangetic Plain, rice, wheat, other cereals, and millet are cultivated in the respective seasons corresponding to the change between wet and dry climatic conditions. Therefore, seasonal variations in the atmospheric CO<sub>2</sub> mole fraction were strongly influenced by the crop CO<sub>2</sub> sink at that time. In general, low CO<sub>2</sub> mole fractions in the winter season in the Northern Hemisphere were not observed, however, we observed relatively lower mole fractions during January–March in this region, especially at CLA. In Bangladesh, rice is grown even in the winter season. The δ<sup>13</sup>C-CO<sub>2</sub> signature showed C<sub>3</sub> plants (e.g., rice and wheat) affected the CO<sub>2</sub> mole fractions in the winter season, while in the summer season the δ<sup>13</sup>C-CO<sub>2</sub> signature showed C<sub>4</sub> plants (corn, sugar cane etc.) contributed some portion.

The seasonal variations in δ<sup>18</sup>O-CO<sub>2</sub> showed almost the same variation as that in the δ<sup>18</sup>O in local rain. Effects of the amount of precipitation and the origin of moisture, appeared to affect δ<sup>18</sup>O in local rain and CO<sub>2</sub>. As a result, δ<sup>18</sup>O in CO<sub>2</sub> was affected by the climatic variation related to the amount of precipitation, which was enhanced during 2015–2017. These facts are also consistent with the explanation that CO<sub>2</sub> exchange by photosynthesis (and respiration) by land biomass strongly affected CO<sub>2</sub> seasonality in mole fraction.

At both sites, higher CH<sub>4</sub> mole fractions were observed than were recorded at other Indian sites. Especially, higher mole fractions than 4000 ppb were recorded at CLA, where rice paddy fields covered the area. Rice cultivation was one of



major emission sources in this region. Because  $\text{CH}_4$  production activities increased after rice planting, we observed the highest peak in September–October at both sites and a small peak in spring at CLA. A large amount of precipitation during those seasons is likely to have affected the  $\text{CH}_4$  production rate of rice paddy fields through soil anaerobic conditions and, as a result, increased the atmospheric  $\text{CH}_4$  mole fraction. Air mass transport also influenced seasonal variation and the variability of its growth rate. Beside emissions from rice paddy fields, we identified the relationship between biomass burning and the  $\text{CH}_4$  mole fraction in a season other than September–October, when biomass burning occurred frequently. In addition, enteric fermentation and wastewater handling were large emission sources in this region. The large number of sources appeared to increase the average  $\text{CH}_4$  mole fraction in this region.

$\text{CO}$  was strongly related to biomass burning activities at both sites. The mole fraction was high in the dry season and after crop harvesting. At CLA in winter, a higher mole fraction was observed together with a high  $\text{N}_2\text{O}$  mole fraction, which may suggest some link to biomass burning as a  $\text{N}_2\text{O}$  source. The  $\text{CO}$  level gradually decreased throughout the observed period.  $\text{CO}$  emissions must, therefore, be reduced by various technical progresses including automobile emission and industrial combustion efficiency improvements.

We observed higher  $\text{N}_2\text{O}$  levels in the crop season (i.e., the rainy season) from May–September at NTL, but much higher levels in the winter season at CLA.  $\text{N}_2\text{O}$  is known to be mainly emitted from soil through nitrogen fertilizer applications to rice fields and crop lands in this region. However, for CLA, we estimated seasonal variations in the emission rate due to the water level in the rice paddy field, because intermittent irrigation in winter generally produces more  $\text{N}_2\text{O}$  than continuously flooded conditions in the rainy season.

$\text{H}_2$  showed some relationship to both  $\text{CO}$  and  $\text{CH}_4$  mole fractions. We found that  $\text{CO}$  had a good correlation with  $\text{H}_2$  in the biomass burning season, indicating some  $\text{H}_2$  contribution from biomass burning. On the other hand, in the season when the  $\text{CH}_4$  mole fraction was high, the  $\text{H}_2$  mole fraction was also relatively high compared to  $\text{CH}_4$ , suggesting that chemical reactions of  $\text{CH}_4$  and  $\text{H}_2$  may contribute some portion of the  $\text{H}_2$  mole fraction.

$\text{SF}_6$  showed consistent mole fractions with other Indian sites. Seasonal variations were strongly related to the southern air mass frequency, because the  $\text{SF}_6$  mole fraction in the southern region was relatively low.

We found that the interannual variabilities in  $\text{CH}_4$ ,  $\text{SF}_6$  and also partly in  $\text{CO}_2$ , growth rates at NTL were anticorrelated with those at MLO, which is located in the Pacific. Growth rates for many GHGs are known to be influenced by El Niño events for many reasons (e.g., hot climate, dry conditions on a global scale). However, in the Indian region, growth rates of some GHGs seemed to be more affected by the regional climate condition, which usually affects air circulation and precipitation in the Indian region. In the case of CLA, although the data duration was insufficiently short, growth rates of  $\text{CO}_2$ ,  $\text{CH}_4$ , and  $\text{SF}_6$  changed differently from those at MLO, which could be partly explained by the climatic variations. Because CLA is located relatively close to the ocean, sometimes the variation was thought to be different from that at NTL.

These findings have not been reported previously. In this study, long-term records of GHGs data at NTL enabled a long-term analysis. These findings suggested that the mole fractions of GHGs and their emissions on the Indian subcontinent could change with climatic conditions in this region in the near future, in addition to changes in anthropogenic activities relating to GHG emissions and countermeasure for the emissions. Therefore, long-term GHG monitoring should be continued and the effectiveness of countermeasures for reducing GHG emissions on the Indian subcontinent, including the Indo-Gangetic Plain, should be evaluated.

## 5. Data availability

We will add digital object identifiers (DOIs) to weekly flask sampling data of Nainital and Comilla and those data on our website (<http://db.cger.nies.go.jp/portal/geds/atmosphericAndOceanicMonitoring>) by 2021.



## 655 Conflicts of Interest

656 The authors declare no conflicts of interest.

## 657 Acknowledgments

658 We would like to thank Deepak Singh Chausali and other staff of the Aryabhata Research Institute of Observational  
 659 Sciences (ARIES), and the staff of Comilla weather station in Bangladesh Meteorological Department (BMD) for their great  
 660 support in this project. The establishment and running of the air sampling program were partly supported by the Asia Pacific  
 661 Network (grant ARCP2011-11NMY-Patra/Canadell), and the Environment Research and Technology Development Fund  
 662 (JPMEERF20152002 and JPMEERF20182002) of the Ministry of the Environment, Japan and the Environmental Restoration  
 663 and Conservation Agency of Japan. We thank Pieter Tans, Ed. Dlugokencky, Paul. C. Novelli Geoff. Dutton, Bradley Hall  
 664 and the Earth System Research Laboratory team of the National Oceanic and Atmospheric Administration (NOAA), and James  
 665 White, Bruce Vaughn and Sylvia Michel and the Institute of Arctic and Alpine Research team of the University of Colorado  
 666 for providing the data of Mauna Loa Observatory.

## 667 References

- 668 Akagi, S. K., Yokelson, R. J., Wiedinmyer, C., Alvarado, M. J., Reid, J. S., Karl, T., Crounse, J. D., and Wennberg, P. O.:  
 669 Emission factors for open and domestic biomass burning for use in atmospheric models. *Atmospheric Chemistry and*  
 670 *Physics*, 11(9), 4039-4072, 2011.
- 671 Akiyama, H., Yagi, K., and Yan, X.: Direct N<sub>2</sub>O emissions from rice paddy fields: summary of available data. *Global*  
 672 *Biogeochemical Cycles*, 19(1), 2005.
- 673 Ali, M. A., Farouque, M. G., Haque, M., and ul Kabir, A.: Influence of soil amendments on mitigating methane emissions and  
 674 sustaining rice productivity in paddy soil ecosystems of Bangladesh. *Journal of Environmental Science and Natural*  
 675 *Resources*, 5(1), 179-185, 2012.
- 676 Andreae, M. O., and Merlet, P.: Emission of trace gases and aerosols from biomass burning. *Global biogeochemical*  
 677 *cycles*, 15(4), 955-966, 2001.
- 678 Arino, O., Perez, R. J., Julio, Kalogirou V., Bontemps S., Defourny P., and Van Bogaert E.: Global land cover map for 2009  
 679 (GlobCover 2009), European Space Agency (ESA) & Université catholique de Louvain (UCL), 2012. [Available  
 680 at <http://www.esa-landcover-cci.org/>]
- 681 Ashok, K., Guan, Z., Saji, N. H., and Yamagata, T.: Individual and combined influences of ENSO and the Indian Ocean dipole  
 682 on the Indian summer monsoon. *Journal of Climate*, 17(16), 3141-3155, 2004.
- 683 Asoka, A., Gleeson, T., Wada, Y., and Mishra, V.: Relative contribution of monsoon precipitation and pumping to  
 684 changes in groundwater storage in India. *Nature Geoscience*, 10(2), 109-117, 2017.
- 685 Begum, K., Kuhnert, M., Yeluripati, J. B., Ogle, S. M., Parton, W. J., Williams, S. A., Pan, G., Cheng, K., Ali, M. A. and  
 686 Smith, P.: Modelling greenhouse gas emissions and mitigation potentials in fertilized paddy rice fields in  
 687 Bangladesh. *Geoderma*, 341, 206-215, 2019.
- 688 Bhatia, A., Ghosh, A., Kumar, V., Tomer, R., Singh, S. D., and Pathak, H.: Effect of elevated tropospheric ozone on methane  
 689 and nitrous oxide emission from rice soil in north India. *Agriculture, ecosystems and environment*, 144(1), 21-28, 2011.
- 690 Bhattacharya, S. K., Borole, D. V., Francey, R. J., Allison, C. E., Steele, L. P., Krummel, P., Langenfelds, R., Masarie, K. A.,  
 691 Tiwari, Y. K., and Patra, P. K.: Trace gases and CO<sub>2</sub> isotope records from Cabo de Rama, India, *Curr. Sci.*, 97, 1336-1344,  
 692 2009.



- Brand, W. A., Assonov, S. S., and Coplen, T. B.: Correction for the  $^{17}\text{O}$  interference in  $\delta(^{13}\text{C})$  measurements when analyzing  $\text{CO}_2$  with stable isotope mass spectrometry (IUPAC Technical Report). *Pure and Applied Chemistry*, 82(8), 1719-1733, 2010.
- Breitenbach, S. F. M., Adkins, J. F., Meyer, H., Marwan, N., Kumar, K. K., and Haug, G. H.: Strong influence of water vapor source dynamics on stable isotopes in precipitation observed in Southern Meghalaya, NE India, *Earth Planet Sci. Lett.*, 292, 212-220, 2010.
- Chandra, N., Lal, S., Venkataramani, S., Patra, P. K., and Sheel, V.: Temporal variations of atmospheric  $\text{CO}_2$  and CO at Ahmedabad in western India, *Atmos. Chem. Phys.*, 16, 6153–6173, doi:10.5194/acp-16-6153-2016, 2016.
- DAC/MA.: Agricultural Statistics at a Glance 2014, Directorate of Economics and Statistics, Department of Agriculture and Cooperation (DAC), Ministry of Agriculture (MA), Government of India, Oxford Univ. Press, New Delhi, India, 2015.
- DES/MAFW.: Crop Production Statistics for Selected States, Crops and Range of Year, Directorate of Economics and Statistics (DES), Ministry of Agriculture and Farmers Welfare (MAFW), Government of India.
- [https://aps.dac.gov.in/APY/Public\\_Report1.aspx](https://aps.dac.gov.in/APY/Public_Report1.aspx) (accessed 2019-July-31), 2019.
- Dickerson, R. R., Andreae, M. O., Campos, T., Mayol - Bracero, O. L., Neusuess, C., and Streets, D. G.: Analysis of black carbon and carbon monoxide observed over the Indian Ocean: Implications for emissions and photochemistry. *Journal of Geophysical Research: Atmospheres*, 107(D19), 2002.
- EC-JRC/PBL.: EDGAR v4.3.2 (1970 - 2012) on March 2016, Emissions Database for Global Atmospheric Research (EDGAR), European Commission, Joint Research Centre (EC-JRC), Netherlands Environmental Assessment Agency (PBL), <http://edgar.jrc.ec.europa.eu>, 2016.
- Friedlingstein, P., Jones, M. W., O'Sullivan, M., Andrew, R. M., Hauck, J., Peters, G. P., et al.: Global carbon budget 2019, *Earth System Science Data*, 11(4), 1783–1838. <https://doi.org/10.5194/essd-11-1783-2019>, 2019.
- Gaihre, Y. K., Singh, U., Islam, S. M., Huda, A., Islam, M. R., Sanabria, J., Satter, M. A., Islam, M. R., Biswas, J. C., Jahiruddin, M., and Jahan, M. S.: Nitrous oxide and nitric oxide emissions and nitrogen use efficiency as affected by nitrogen placement in lowland rice fields. *Nutrient cycling in agroecosystems*, 110(2), 277-291, 2018.
- Ganesan, A. L., Chatterjee, A., Prinn, R. G., Harth, C. M., Salameh, P. K., Manning, A. J., Hall, B. D., Mühle, J., Meredith, L. K., Weiss, R. F., O'Doherty, S., and Young, D.: The variability of methane, nitrous oxide and sulfur hexafluoride in Northeast India, *Atmos. Chem. Phys.*, 13, 10633–10644, doi:10.5194/acp-13-10633-2013, 2013.
- Garg, A., Kankal, B., and Shukla, P. R.: Methane emissions in India: Sub-regional and sectoral trends, *Atmospheric Environment*, 45(28), 4922-4929, 2011.
- Garg, A., Shukla, P. R., and Upadhyay, J.:  $\text{N}_2\text{O}$  emissions of India: an assessment of temporal, regional and sector trends, *Clim. Change*, 110, 755-782, doi:10.1007/s10584-011-0094-9, 2012.
- Geller, L. S., Elkins, J. W., Lobert, J. M., Clarke, A. D., Hurst, D. F., Butler, J. H., and Myers, R. C.: Tropospheric  $\text{SF}_6$ : observed latitudinal distribution and trends, derived emissions and interhemispheric exchange time, *Geophys. Res. Lett.*, 24, 675–678, 1997.
- Gupta, D. K., Bhatia, A., Kumar, A., Das, T. K., Jain, N., Tomer, R., Sandeep, k. M., Fagodiya, R. K., Dubey, R., and Pathak, H.: Mitigation of greenhouse gas emission from rice–wheat system of the Indo-Gangetic Plain: Through tillage, irrigation and fertilizer management. *Agriculture, Ecosystems and Environment*, 230, 1-9, 2016.
- Guttikunda, S., Begum, B., and Wadud, Z.: Particulate pollution from brick kiln clusters in the Greater Dhaka region, Bangladesh. *Air Quality, Atmosphere and Health*, 1e9, 2012.
- Hong, C. C., Li, T., and Kug, J. S.: Asymmetry of the Indian Ocean dipole. Part I: observational analysis. *Journal of climate*, 21(18), 4834-4848, 2008.
- IAEA: Reference and comparison materials for light isotopes of light elements, Proceedings of a consultants meeting held in Vienna, IAEA-TECDOC-825, 1993.



- 736 Keeling, C. D.: Rewards and penalties of monitoring the Earth. *Annual Review of Energy and the Environment*, 23(1), 25-  
 737 82, 1998.
- 738 Kim S. Coplen, T. B. and Horita J.: Normalization of stable isotope data for carbonate minerals: Implementation of IUPAC  
 739 guidelines. *Geochimica et Cosmochimica Acta*, 158, 276-289, 2015.
- 740 Kumar, A., Sanyal, P., and Agrawal, S.: Spatial distribution of  $\delta^{18}\text{O}$  values of water in the Ganga river basin: Insight into the  
 741 hydrological processes, *Journal of Hydrology*, 571, 225-234, 2019.
- 742 Kumar, R., Naja, M., Satheesh, S. K., Ojha, N., Joshi, H., Sarangi, T., Pant, P., Dumka, U. C. Hegde, P. and Venkataramani,  
 743 S.: Influences of the springtime northern Indian biomass burning over the central Himalayas. *Journal of Geophysical*  
 744 *Research: Atmospheres*, 116(D19), 2011.
- 745 Kumar, R., Naja, M., Pfister, G. G., Barth, M. C., and Brasseur, G. P.: Source attribution of carbon monoxide in India and  
 746 surrounding regions during wintertime. *Journal of Geophysical Research: Atmospheres*, 118(4), 1981-1995, 2013.
- 747 Lawrence, M. G., and Lelieveld, J.: Atmospheric pollutant outflow from southern Asia: a review. *Atmospheric Chemistry*  
 748 *and Physics*, 10(22), 11017, 2010.
- 749 Lin, X., Indira, N. K., Ramonet, M., Delmotte, M., Ciais, P., Bhatt, B. C., Reddy, M. V., Angchuk, D., Balakrishnan, S.,  
 750 Jorphail, S., Dorjai, T., Mahey, T. T., Patnaik, S., Begum, M., Brenninkmeijer, C., Durairaj, S., Kirubakaran, R.,  
 751 Schmidt, M., Swathi, P. S., Vinithkumar, N. V., Yver Kwok, C., and Gaur, V. K.: Long-lived atmospheric trace gases  
 752 measurements in flask samples from three stations in India. *Atmos. Chem. Phys.*, 15, 9819–9849, doi:10.5194/acp-15-  
 753 9819-2015, 2015.
- 754 Lohan, S. K., Jat, H. S., Yadav, A. K., Sidhu, H. S., Jat, M. L., Choudhary, M., Peter, J. D. and Sharma, P. C.: Burning issues  
 755 of paddy residue management in north-west states of India. *Renewable and Sustainable Energy Reviews*, 81, 693-706,  
 756 2018.
- 757 Maithel, S., Uma, R., Bond, T., Baum, E., and Thao, V. T. K.: Brick kilns performance assessment, emissions measurements,  
 758 and a roadmap for cleaner brick production in India. Study report prepared by Green Knowledge Solutions, New Delhi,  
 759 2012.
- 760 Mukai H.: NIES pure  $\text{CO}_2$  sample for inter-laboratory comparison of C and O isotope ratio analysis especially for atmospheric  
 761  $\text{CO}_2$ , proceeding of the 11<sup>th</sup> WMO/IAEA Meeting of Experts on Carbon Dioxide Mole fraction and Related Tracer  
 762 Measurement Techniques. In: WMO/GAW Rep, 31, 2001.
- 763 Mukai H.: Inter-Comparison of Isotope Ratios For  $\text{CO}_2$  Using Several Reference Materials, proceeding of the 12<sup>th</sup>  
 764 WMO/IAEA Meeting of Experts on Carbon Dioxide Mole fraction and Related Tracer Measurement Techniques, In:  
 765 WMO/GAW Rep, 58–62, 2003.
- 766 Naja, M., Bhardwaj, P., Singh, N., Kumar, P., Kumar, R., Ojha, N., ... & Kotamarthi, V. R.: High-frequency vertical profiling  
 767 of meteorological parameters using AMF1 facility during RAWEX–GVAX at ARIES, Nainital, *Corrent Science*, 111(1),  
 768 132-140, 2016.
- 769 Nayak, R. K., Patel, N. R., and Dadhwal, V. K.: Estimation and analysis of terrestrial net primary productivity over India by  
 770 remote-sensing-driven terrestrial biosphere model, *Environ. Monit. Assess.*, 170, 195–213, doi:10.1007/s10661-009-1226-  
 771 9, 2010.
- 772 NOAA/ESRL.: The 6<sup>th</sup> WMO/IAEA Round Robin Comparison Experiment.  
 773 [http://www.esrl.noaa.gov/gmd/ccgg/wmorrr/wmorrr\\_results.php?rr=rr6&param=co2&group=group5](http://www.esrl.noaa.gov/gmd/ccgg/wmorrr/wmorrr_results.php?rr=rr6&param=co2&group=group5) (accessed 2019-May.-  
 774 15), 2019a.
- 775 NOAA/ESRL.: ESRL/GMD FTP Data Finder. <https://www.esrl.noaa.gov/gmd/dv/data/> (accessed 2019-May.-15), 2019b.
- 776 NOAA/ESRL.: Dipole Mode Index. [https://www.esrl.noaa.gov/psd/gcos\\_wgsp/Timeseries/DMI/](https://www.esrl.noaa.gov/psd/gcos_wgsp/Timeseries/DMI/) (accessed 2021a-Apr.-6),  
 777 2021.
- 778 NOAA/ESRL.: Multivariate ENSO Index. <https://www.esrl.noaa.gov/psd/enso/mei/> (accessed 2021-Apr.-6), 2021b.



- 779 Novelli, P. C., Lang, P. M., Masarie, K. A., Hurst, D. F., Myers, R., and Elkins, J. W.: Molecular hydrogen in the troposphere:  
 780 Global distribution and budget, *J. Geophys. Res. Atmos.*, 104, 30427–30444, 1999.
- 781 Olivier, J. G. J., Van Aardenne, J. A., Dentener, F., Ganzeveld, L., and Peters J. A. H. W.: Recent trends in global  
 782 greenhouse gas emissions: regional trends and spatial distribution of key sources, in: *Non-CO<sub>2</sub> Greenhouse Gases*  
 783 (NCGG-4), edited by: Van Amstel, A., 325–330, Millpress, Rotterdam, The Netherlands, 2005.
- 784 Pandey, A. K., Mishra, A. K., Kumar, R., Berwal, S., Devadas, R., Huete, A., and Kumar, K.: CO variability and its  
 785 association with household cooking fuels consumption over the Indo-Gangetic Plain. *Environmental pollution*, 222, 83–  
 786 93, 2017.
- 787 Panigrahy, S., Upadhyay, G., Ray, S. S., and Parihar, J. S.: Mapping of cropping system for the Indo-Gangetic Plain using  
 788 multi-date SPOT NDVI-VGT Data, *J. Indian Soc. Remote Sens.*, 38(4), 627–632, doi:10.1007/s12524-011-0059-5, 2010.
- 789 Price, H., Jaegle, L., Rice, A., Quay, P., Novelli, P. C., and Gammon, R.: Global budget of molecular hydrogen and its  
 790 deuterium content: Constraints from ground station, cruise, and aircraft observations, *J. Geophys. Res.*, 112, D22108,  
 791 doi:10.1029/2006JD008152, 2007.
- 792 Raut, N., Sitaula, B. K., and Bajracharya, R. M.: Agricultural intensification in South Asia and its contribution to greenhouse  
 793 gas emission: A review, *Asian Journal of water, environment and pollution*, 8(3), 11–17, 2011.
- 794 Roxy, M. K., Ritika, K., Terray, P., Murtugudde, R., Ashok, K., and Goswami, B. N.: Drying of Indian subcontinent by rapid  
 795 Indian Ocean warming and a weakening land-sea thermal gradient, *Nature communications*, 6, 7423, 2015.
- 796 Rozanski, K., Araguás - Araguás, L., and Gonfiantini, R.: Isotopic patterns in modern global precipitation, in *Climate change*  
 797 *in continental isotopic records*, *Geophys. Monogr. Ser.*, vol. 78, edited by P. K. Swart et. al., pp. 1–36, AGU, Washington,  
 798 D. C., 1993.
- 799 Sahai, S., Sharma, C., Singh, D. P., Dixit, C. K., Singh, N., Sharma, P., Singh, K., Bhatt, S., Ghude, S., Gupta, V., Gupta, R.  
 800 K., Tiwari, M. K., Garg, S. C., Mitra, A. P. and Gupta, R. K.: A study for development of emission factors for trace gases  
 801 and carbonaceous particulate species from in situ burning of wheat straw in agricultural fields in India. *Atmospheric*  
 802 *Environment*, 41(39), 9173–9186, 2007.
- 803 Sahai, S., Sharma, C., Singh, S.K., and Gupta, P.K.: Assessment of trace gases, carbon and nitrogen emissions from field  
 804 burning of agricultural residues in India. *Nutrient Cycling in Agroecosystems* 89, 143e157, 2011.
- 805 Saji, N. H., Goswami, B. N., Vinayachandran, P. N., and Yamagata, T.: A dipole mode in the tropical Indian  
 806 Ocean. *Nature*, 401(6751), 360, 1999.
- 807 Sengupta, S. and Sarkar, A.: Stable isotope evidence of dual (Arabian Sea and Bay of Bengal) vapour sources in monsoonal  
 808 precipitation over north India. *Earth Planet. Sci. Lett.* 250, 511–521, 2006.
- 809 Sfez, S., De Meester, S., and Dewulf, J.: Co-digestion of rice straw and cow dung to supply cooking fuel and fertilizers in rural  
 810 India: Impact on human health, resource flows and climate change. *Science of the Total Environment*, 609, 1600–1615,  
 811 2017.
- 812 Sharma, A. R., Kharol, S. K., Badarinath, K. V. S., Singh, D.: Impact of agriculture crop residue burning on atmospheric  
 813 aerosol loading — a study over Punjab State, India. *Ann. Geophys.* 28, 367–379, 2010.
- 814 Sharma, N., Nayak, R. K., Dadhwal, V. K., Kant, Y., and Ali, M. M.: Temporal variations of atmospheric CO<sub>2</sub> in Dehradun,  
 815 India during 2009, *Air Soil Water Res.*, 6, 37–45, 2013.
- 816 SID/MP.: Statistical Year Book Bangladesh 2018, Statistics and Informatics Division (SID), Ministry of Planning (MP),  
 817 Government of the people's republic of Bangladesh, Dhaka, Bangladesh, 2018.
- 818 Sreenivas, G., Mahesh, P., Subin, J., Kanchana, A. L., Rao, P. V. N., and Dadhwal, V. K.: Influence of Meteorology and  
 819 interrelationship with greenhouse gases (CO<sub>2</sub> and CH<sub>4</sub>) at a suburban site of India, *Atmos. Chem. Phys.*, 16, 3953–3967.  
 820 doi:10.5194/acp-16-3953-2016, 2016.





- Streets, D. G., Yarber, K. F., Woo, J.-H., and Carmichael, G. R.: Biomass burning in Asia: Annual and seasonal estimates and atmospheric emissions, *Global Biogeochem. Cy.*, 17, 1099, doi:10.1029/2003GB002040, 2003.
- Swapna, P., Krishnan, R., and Wallace, J. M.: Indian Ocean and monsoon coupled interactions in a warming environment, *Climate dynamics*, 42(9-10), 2439-2454, 2014.
- Tanoue, M., Ichianagi, K., Yoshimura, K., Kiguchi, M., Terao, T., and Hayashi, T.: Seasonal variation in isotopic composition and the origin of precipitation over Bangladesh, *Progress in Earth and Planetary Science*, 5-77, 2018.
- Thompson, R. L., Ishijima, K., Saikawa, E., Corazza, M., Karstens, U., Patra, P. K., Bergamaschi, P., Chevallier, F., Dlugokencky, E., Prinn, R. G., Weiss, R. F., O'Doherty, S., Fraser, P. J., Steele, L. P., Krummel, P. B., Vermeulen, A., Tohjima, Y., Jordan, A., Haszpra, L., Steinbacher, M., Van der Laan, S., Aalto, T., Meinhardt, F., Popa, M. E., Moncrieff, J., and Bousquet, P.: TransCom N<sub>2</sub>O model inter-comparison – Part 2: Atmospheric inversion estimates of N<sub>2</sub>O emissions, *Atmos. Chem. Phys.*, 14, 6177–6194, doi:10.5194/acp-14-6177-2014, 2014.
- Thoning, K.W., Tans, P.P. and Komhyr W.D.: Atmospheric carbon dioxide at Mauna Loa Observatory, 2. Analysis of the NOAA GMCC data, 1974–1985. *J. Geophys. Res.*, 94 (D6), 8549–8565, 1989.
- Tiwari, Y. K., Vellore, R. K., Ravi Kumar, K., van der Schoot, M., and Cho, C.-H.: Influence of monsoons on atmospheric CO<sub>2</sub> spatial variability and ground-based monitoring over India, *Sci. Total Environ.*, 490, 570–578, doi:10.1016/j.scitotenv.2014.05.045, 2014.
- Umezawa, T., Niwa, Y., Sawa, Y., Machida, T., and Matsueda, H.: Winter crop CO<sub>2</sub> uptake inferred from CONTRAIL measurements over Delhi, India. *Geophysical Research Letters*, 10.1002/2016GL070939, 11859-11866, 2016.
- Venkataraman, C., Habib, G., Kadamba, D., Shrivastava, M., Leon, J. F., Crouzille, B., Boucher, O., and Streets, D. G.: Emissions from open biomass burning in India: Integrating the inventory approach with high - resolution Moderate Resolution Imaging Spectroradiometer (MODIS) active - fire and land cover data. *Global biogeochemical cycles*, 20(2), 2006.
- Venkataraman, C., Sagar, A. D., Habib, G., Lam, N., and Smith, K. R.: The Indian national initiative for advanced biomass cookstoves: the benefits of clean combustion. *Energy for Sustainable Development*, 14(2), 63-72, 2010.
- WDCGG.: Data/Quick Plot. <http://ds.data.jma.go.jp/gmd/wdogg/cgi-bin/wdogg/accessdata.cgi?index=CRI215N00-CSIRO&select=inventory> (accessed 2017-Dec.-14), 2017.
- Yashiro, H., Sudo, K., Yonemura, S., and Takigawa, M.: The impact of soil uptake on the global distribution of molecular hydrogen: chemical transport model simulation. *Atmospheric Chemistry and Physics*, 11(13), 6701-6719, 2011.
- Zeng, J. and Fujinuma, Y.: New web site launched for online air trajectory calculation. *EOS, Transactions American Geophysical Union* 85(46), 482, 2004.



## 851 Tables

852

853 Table 1. Annual mean atmospheric mole fractions of CO<sub>2</sub>, CH<sub>4</sub>, CO, H<sub>2</sub>, N<sub>2</sub>O, and SF<sub>6</sub> and isotopic ratio of δ<sup>13</sup>C-CO<sub>2</sub> and  
 854 δ<sup>18</sup>O-CO<sub>2</sub> at Nainital (NTL) and Comilla (CLA) in 2007–2020.

Site	Year	CO <sub>2</sub>		CH <sub>4</sub>		CO		H <sub>2</sub>		N <sub>2</sub> O		SF <sub>6</sub>		δ <sup>13</sup> C-CO <sub>2</sub>		δ <sup>18</sup> O-CO <sub>2</sub>	
		ppm		ppb		ppb		ppb		ppb		ppt		‰		‰	
		Ave	S.D	Ave	S.D	Ave	S.D	Ave	S.D	Ave	S.D	Ave	S.D	Ave	S.D	Ave	S.D
Nainital	2007	380.6	9.6	1928.4	70.6	238.7	100.5	546.1	19.7	321.9	0.83	6.25	0.17	-8.14	0.44	0.72	1.09
Nainital	2008	383.2	7.8	1931.0	75.5	225.4	99.4	551.8	24.1	323.0	0.83	6.57	0.29	-8.15	0.35	0.50	1.00
Nainital	2009	383.5	9.3	1919.4	63.3	210.2	79.2	538.8	28.0	323.7	0.88	6.95	0.28	-8.13	0.44	0.55	0.87
Nainital	2010	386.5	9.0	1925.7	59.7	214.4	92.6	537.9	25.6	324.7	0.87	7.19	0.24	-8.19	0.42	0.28	1.13
Nainital	2011	389.6	6.3	1945.2	70.3	213.7	72.1	544.6	24.5	325.4	0.97	7.52	0.21	-8.28	0.32	0.35	1.20
Nainital	2012	391.2	7.5	1956.0	76.7	222.1	79.3	552.6	29.9	326.2	1.18	7.85	0.35	-8.22	0.33	0.31	1.12
Nainital	2013	391.7	8.0	1963.1	58.2	223.2	69.7	549.9	24.8	327.2	1.03	8.11	0.15	-8.19	0.39	0.47	1.29
Nainital	2014	394.3	7.5	1961.2	75.4	205.5	66.0	543.0	22.9	328.3	1.17	8.48	0.16	-8.25	0.34	0.92	0.93
Nainital	2015	396.0	8.3	1984.1	72.8	226.6	77.1	549.3	28.1	329.4	1.02	8.84	0.23	-8.24	0.38	1.04	0.87
Nainital	2016	400.8	8.2	1990.0	62.8	227.6	77.7	557.1	24.1	329.9	0.92	9.05	0.14	-8.36	0.39	0.92	1.10
Nainital	2017	401.6	8.5	2012.1	83.8	229.0	77.8	555.9	26.3	331.0	1.24	9.43	0.16	-8.28	0.41	0.90	1.08
Nainital	2018	404.3	7.8	2013.8	67.9	225.1	82.8	559.7	33.2	332.2	0.95	9.74	0.14	-8.36	0.36	0.91	1.10
Nainital	2019	406.3	8.8	2021.3	64.1	232.4	84.3	556.8	29.5	332.7	1.08	10.10	0.13	-8.36	0.40	0.81	1.19
Nainital	2020	407.4	6.7	2037.3	88.2	206.8	75.0	563.8	48.8	334.0	1.32	10.43	0.17	-8.33	0.31	0.66	1.21
Comilla	2013	393.7	9.0	2214.6	291.6	294.7	168.8	607.7	69.3	328.4	2.29	8.12	0.18	-8.41	0.38	0.42	0.95
Comilla	2014	395.4	10.8	2274.0	402.3	318.6	162.2	612.1	53.7	330.0	2.36	8.46	0.16	-8.44	0.45	0.52	0.82
Comilla	2015	395.6	7.2	2272.4	250.6	293.8	118.4	596.0	32.6	330.5	1.87	8.78	0.13	-8.34	0.32	0.44	0.87
Comilla	2016	402.4	8.1	2363.3	399.5	292.5	119.9	652.5	81.0	330.9	1.75	9.01	0.16	-8.54	0.35	0.11	1.17
Comilla	2017	404.6	8.8	2484.5	450.1	293.4	129.2	601.9	27.6	332.1	2.29	9.37	0.19	-8.54	0.38	-0.14	1.23
Comilla	2018	403.8	8.1	2380.0	253.4	295.7	135.4	669.3	85.6	333.0	1.82	9.68	0.10	-8.47	0.34	0.16	0.86
Comilla	2019	408.9	7.9	2406.7	331.5	284.5	114.0	604.6	36.9	333.9	1.81	10.07	0.16	-8.58	0.33	-0.06	1.44
Comilla	2020	415.2	11.2	2830.6	679.6	339.9	167.4	639.0	91.8	336.0	3.08	10.46	0.24	-8.73	0.50	-0.31	1.15

855  
 856

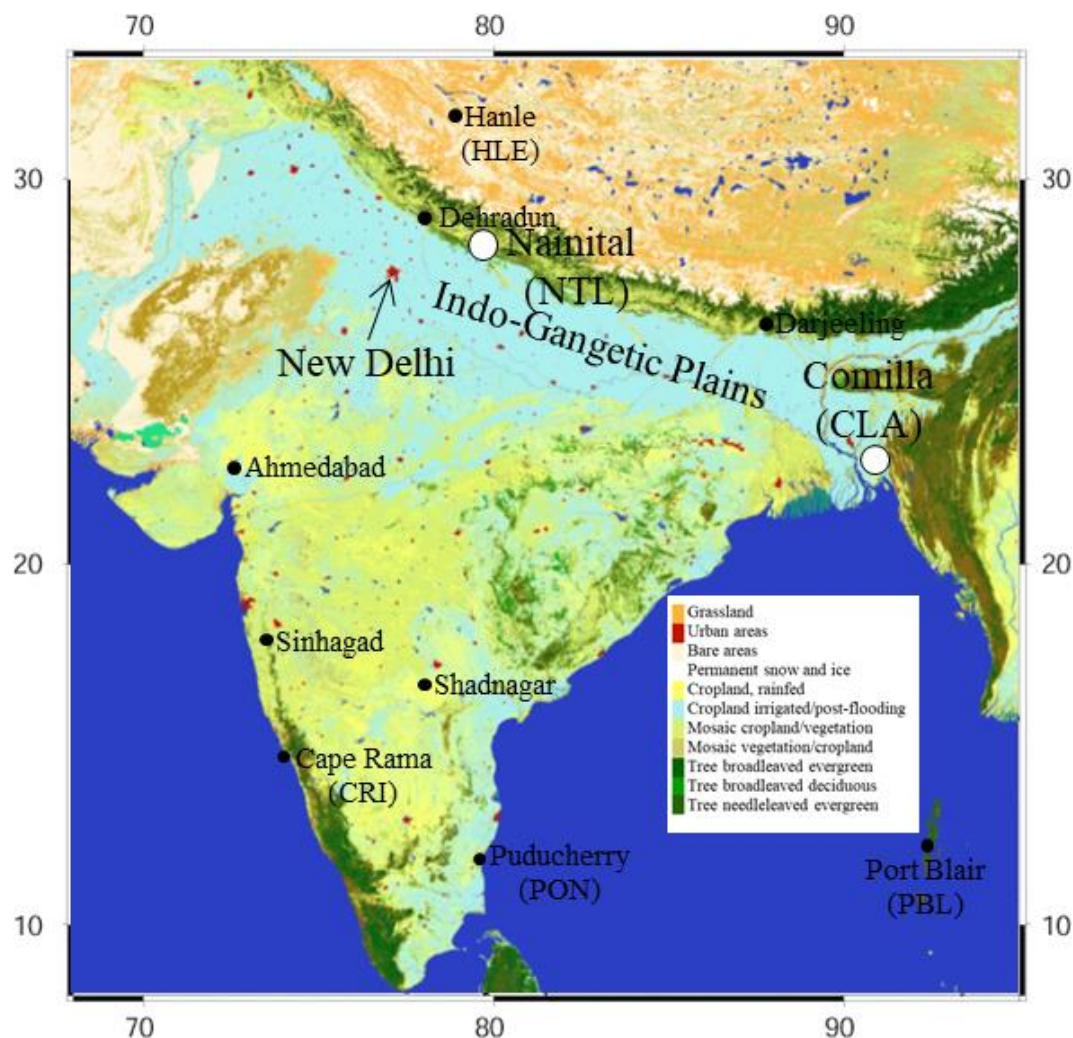


Table 2. Mean annual amplitudes of seasonal variation in atmospheric mole fractions of CO<sub>2</sub>, CH<sub>4</sub>, CO, H<sub>2</sub>, N<sub>2</sub>O, and SF<sub>6</sub> and δ<sup>13</sup>C-CO<sub>2</sub> and δ<sup>18</sup>O-CO<sub>2</sub> at Nainital (NTL) during 2007–2019 and at Comilla (CLA) during 2013–2019.

Site	CO <sub>2</sub> ppm	CH <sub>4</sub> ppb	CO ppb	H <sub>2</sub> ppb	N <sub>2</sub> O ppb	SF <sub>6</sub> ppt	δ <sup>13</sup> C-CO <sub>2</sub> ‰	δ <sup>18</sup> O-CO <sub>2</sub> ‰
Nainital	22.1 ± 3.9	114 ± 52	153 ± 44	50.3 ± 18.0	1.01 ± 0.74	0.18 ± 0.16	0.96 ± 0.16	2.71 ± 0.79
Comilla	20.3 ± 5.7	486 ± 225	356 ± 90	70.4 ± 41.2	4.25 ± 1.45	0.23 ± 0.08	0.85 ± 0.19	2.33 ± 0.49



864



865

866 Figure 1. Location of Nainital (NTL), India (29.36°N, 79.46°E, 1940 m a.s.l.) and Comilla (CLA), Bangladesh (23.43°N,  
 867 91.18°E, 30 m a.s.l.) and other Indian sites for greenhouse gas (GHG) observation (Bhattacharya et al. 2009; Ganesan et al.  
 868 2013; Sharma et al., 2013; Tiwari et al., 2014; Lie et al., 2015; Sreenivas et al., 2016; Chandra et al.; 2016) and showing land  
 869 cover around the South Asia region (Arino et al., 2012).

870

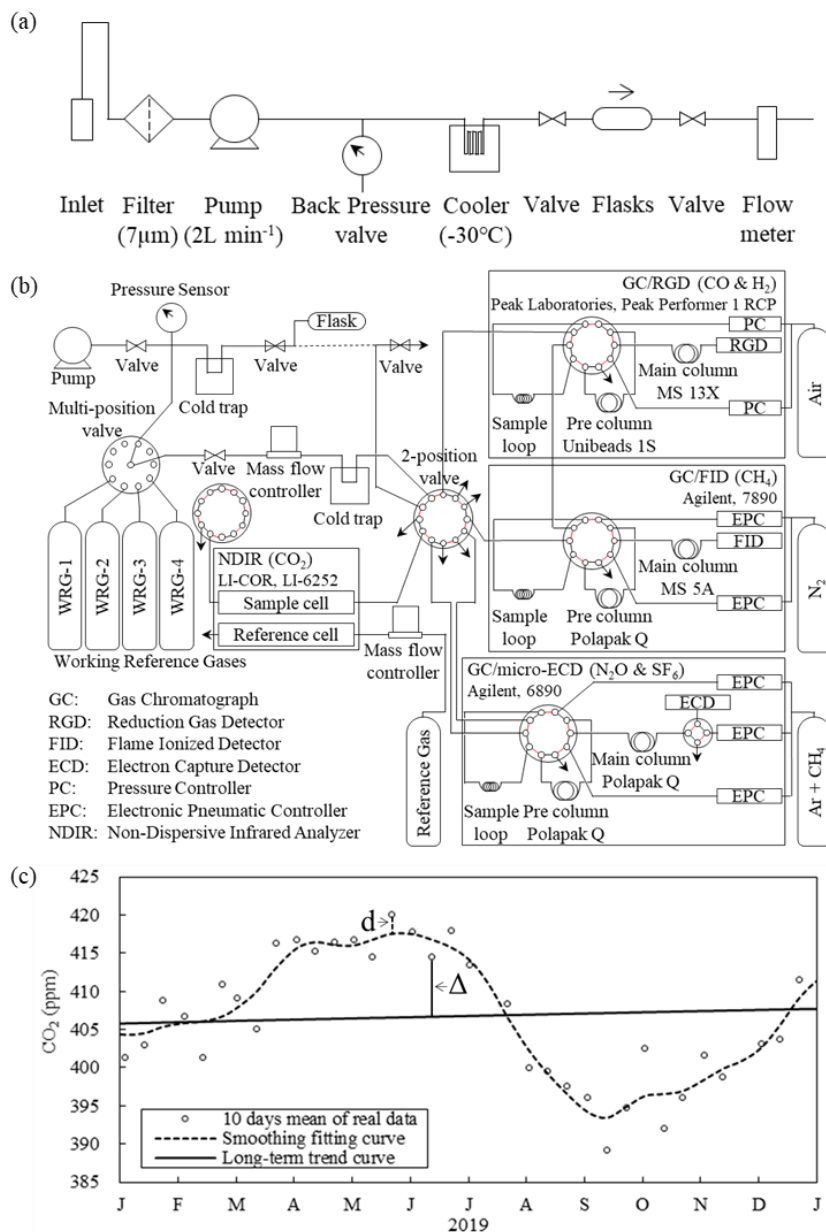
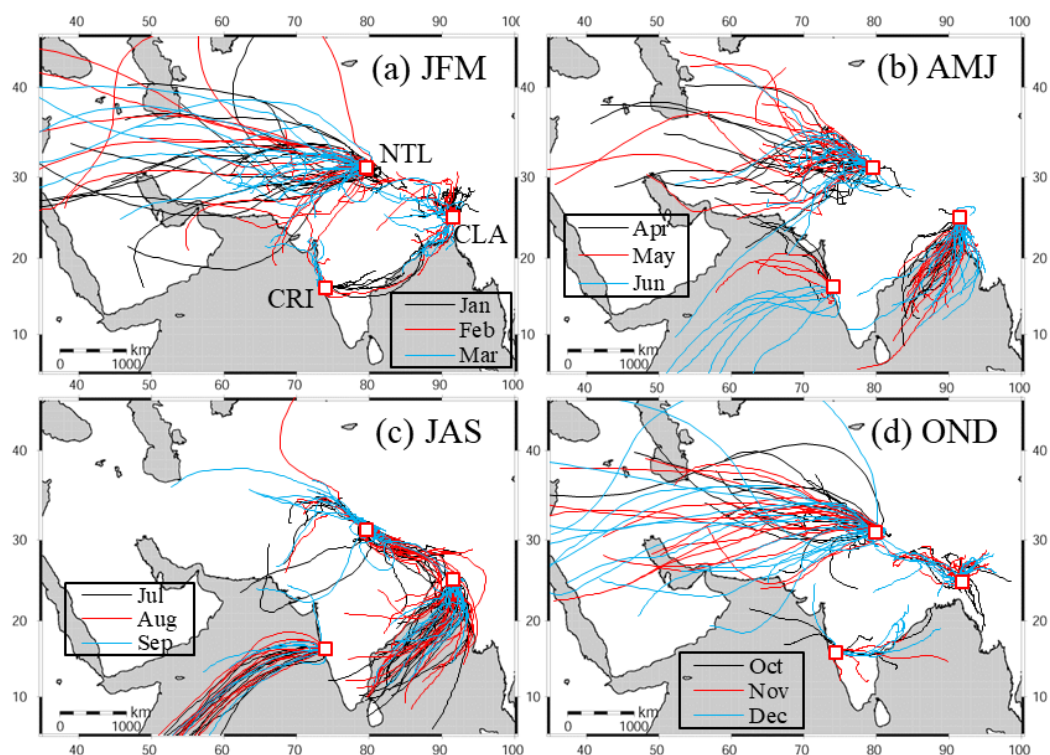


Figure 2. The line used for (a) flask sampling, (b) schematic of measurements of the dry-air mole fraction in the laboratory and (c) diagram of the calculation method for “ $\Delta$ ” term (e.g.,  $\Delta$ CO<sub>2</sub>) which was calculated by subtraction of the long-term trend curve from 10 days mean of real data and “ $d$ ” term (e.g.,  $d$ CO<sub>2</sub>) which was characterized by the deviation of 10 days mean of real data from the smoothing fitting curve.



878



879

880

881 Figure 3. 72-hour back trajectory of Nainital (NTL), Comilla (CLA), and Cape Rama (CRI) in (a) January–March (JFM), (b)  
 882 April–June (AMJ), (c) July–September (JAS), and (d) October–December. 72-hour back trajectory at NTL and CLA showed  
 883 for 2012–2016 and the back trajectory at CRI showed for 2009–2013.

884

885

886



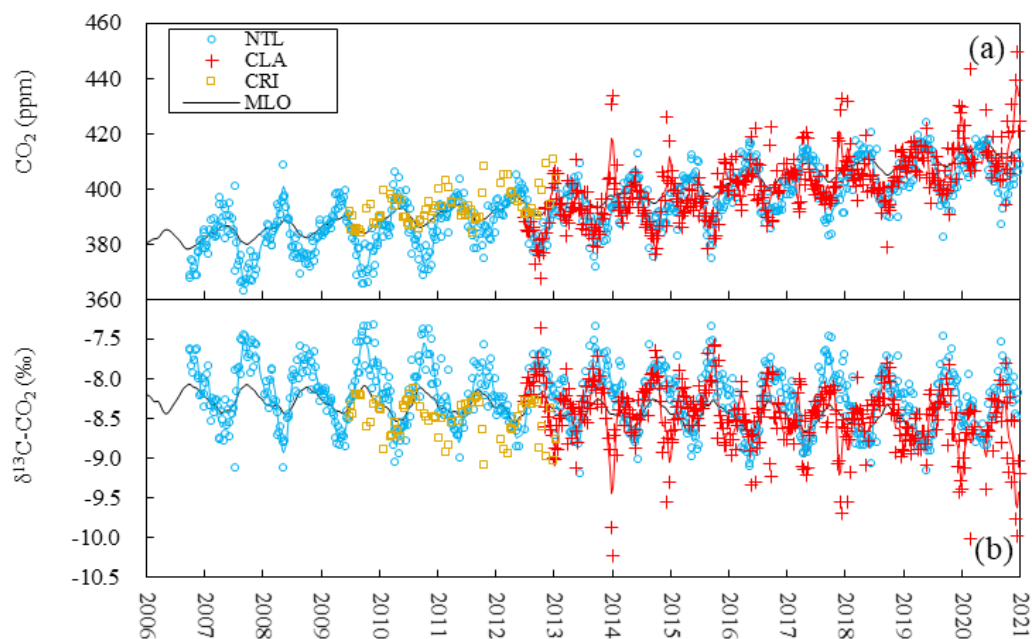
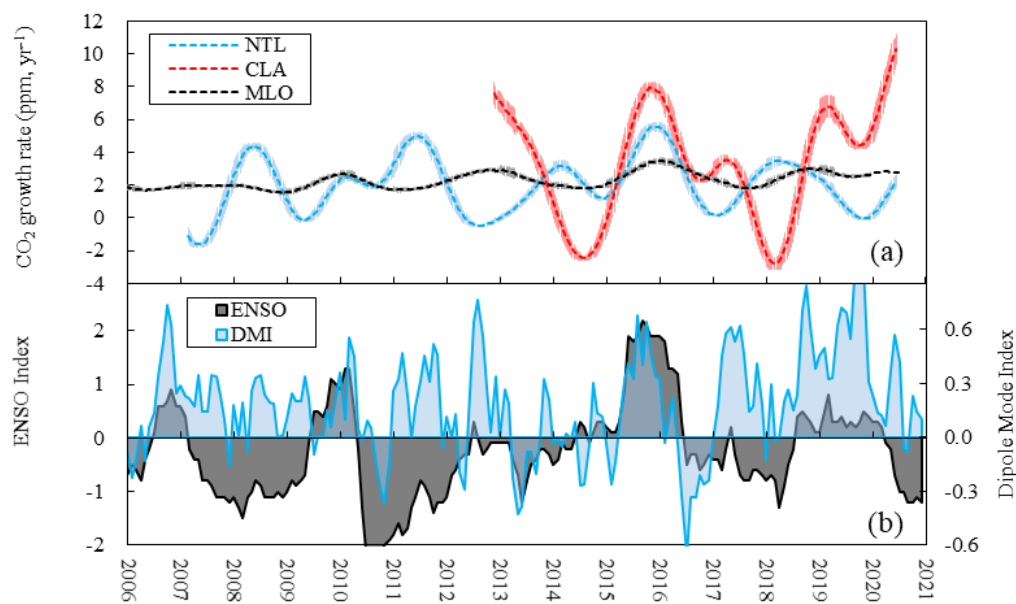


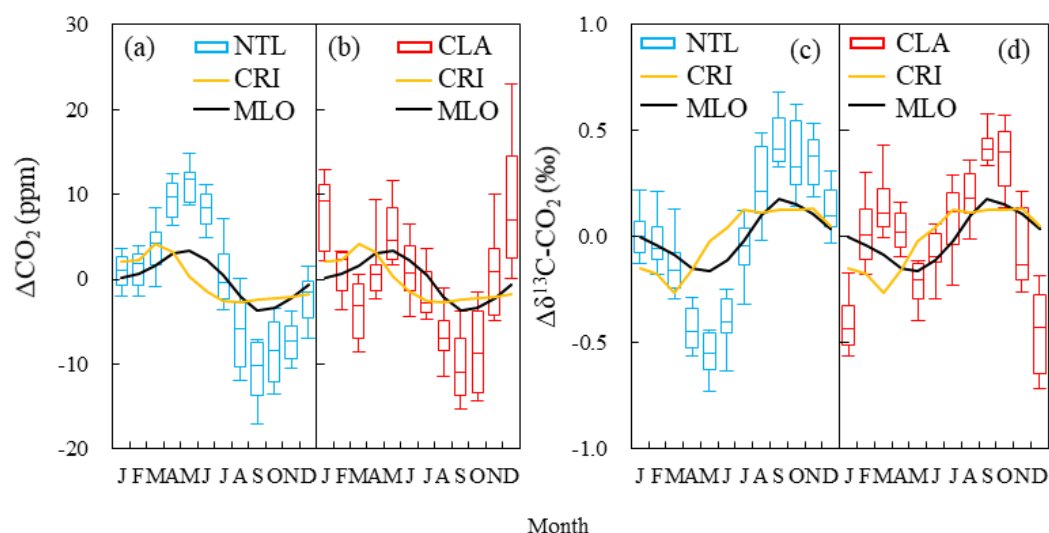
Figure 4. Time series of the (a) atmospheric CO<sub>2</sub> mole fraction, and (b) isotope ratio of δ<sup>13</sup>C-CO<sub>2</sub> at Nainital (NTL), Comilla (CLA), Cape Rama (CRI), and Mauna Loa (MLO) in 2006–2020.



894  
 895  
 896 Figure 5. (a) Growth rates of the CO<sub>2</sub> mole fraction at Nainital (NTL), Comilla (CLA), and Mauna Loa (MLO) in 2006–  
 897 2020, and (b) the El Nino Southern Oscillation (ENSO) Index in 2006–2020 and the Dipole Mode Index (DMI) in 2006–  
 898 2020.  
 899  
 900  
 901



902



903

904

905 Figure 6. Seasonal variations in the CO<sub>2</sub> mole fraction at (a) Nainital (NTL) and (b) Comilla (CLA) and the isotope ratio of  
 906 δ<sup>13</sup>C-CO<sub>2</sub> at (c) NTL and (d) CLA. Boxes with blue and red are for Nainital and Comilla and the black and yellow lines are  
 907 for Mauna Loa (MLO) and Cape Rama (CRI), respectively. Median values (the line in the box), inner 50th percentile of the  
 908 value (box), and inner 90th percentile of the value is from the monthly averaged CO<sub>2</sub> mole fractions.

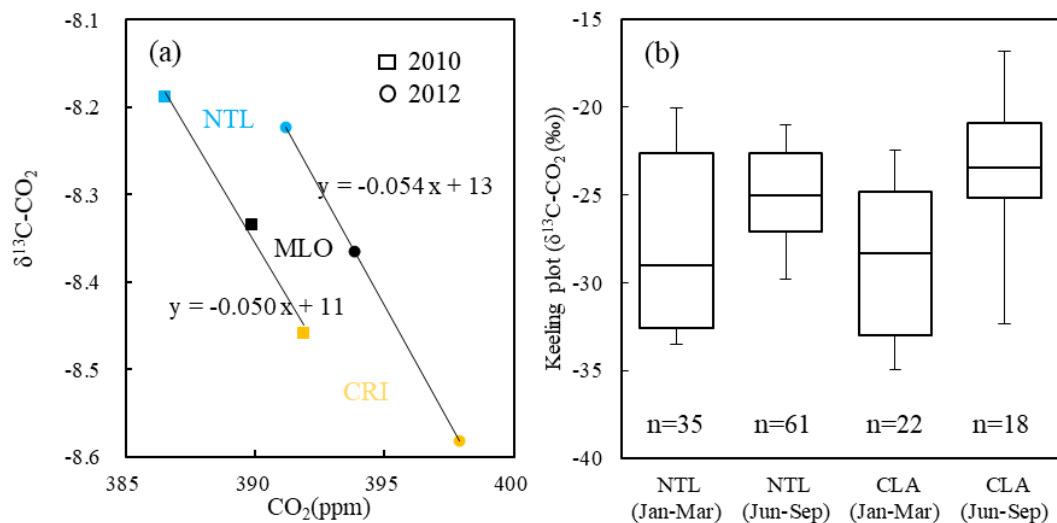
909

910

911



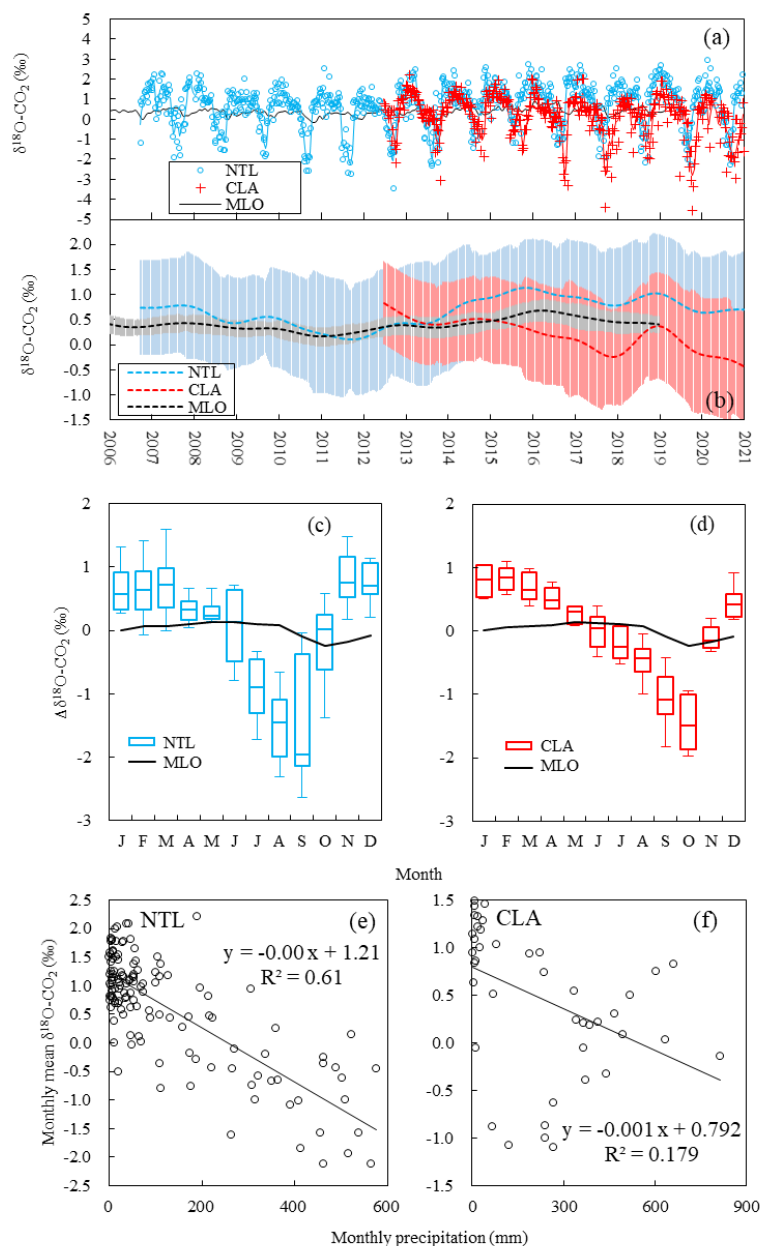
912



913  
 914

915 Figure 7. (a) Relationship between the annual values of the CO<sub>2</sub> mole fraction and isotopic ratio of δ<sup>13</sup>C-CO<sub>2</sub> at Nainital  
 916 (NTL), Cape Rama (CRI), and Mauna Loa (MLO) in 2010 and 2012, and (b) the intercept values of the Keeling plot of  
 917 Nainital and Comilla (CLA) in January–March and June–September.

918  
 919  
 920



921  
 922  
 923 Figure 8. Time series of (a) measured values and (b) long-term trend for isotopic ratio of  $\delta^{18}\text{O}-\text{CO}_2$  at Nainital (NTL),  
 924 Comilla (CLA), and Mauna Loa (MLO) in 2006–2020, the seasonal variation of  $\delta^{18}\text{O}-\text{CO}_2$  at (c) NTL and (d) CLA, and the  
 925 relationship between monthly precipitation of the state of Uttarakhand and Bangladesh and the monthly mean of  $\delta^{18}\text{O}-\text{CO}_2$  at  
 926 (e) NTL and (f) CLA.  
 927  
 928

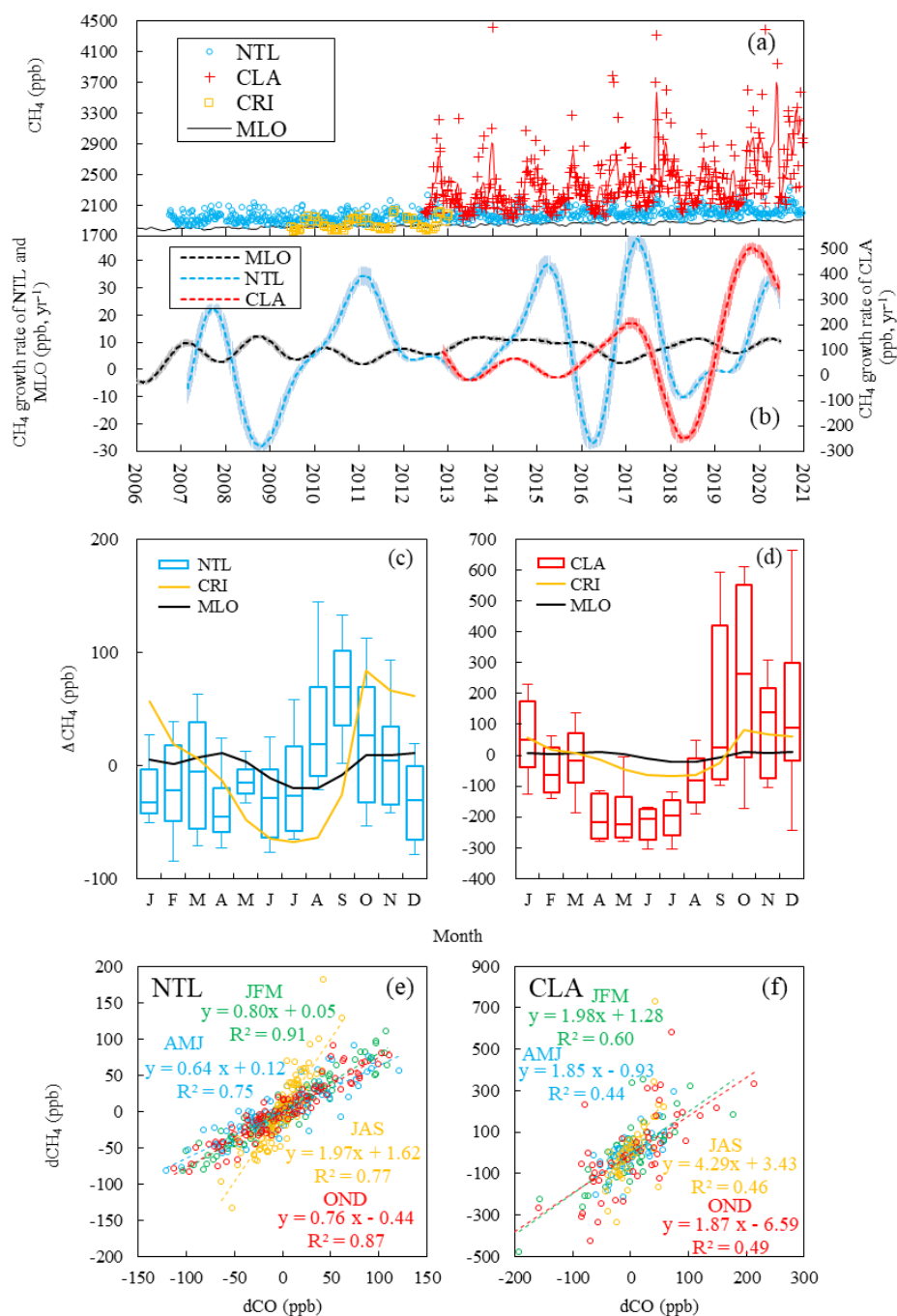
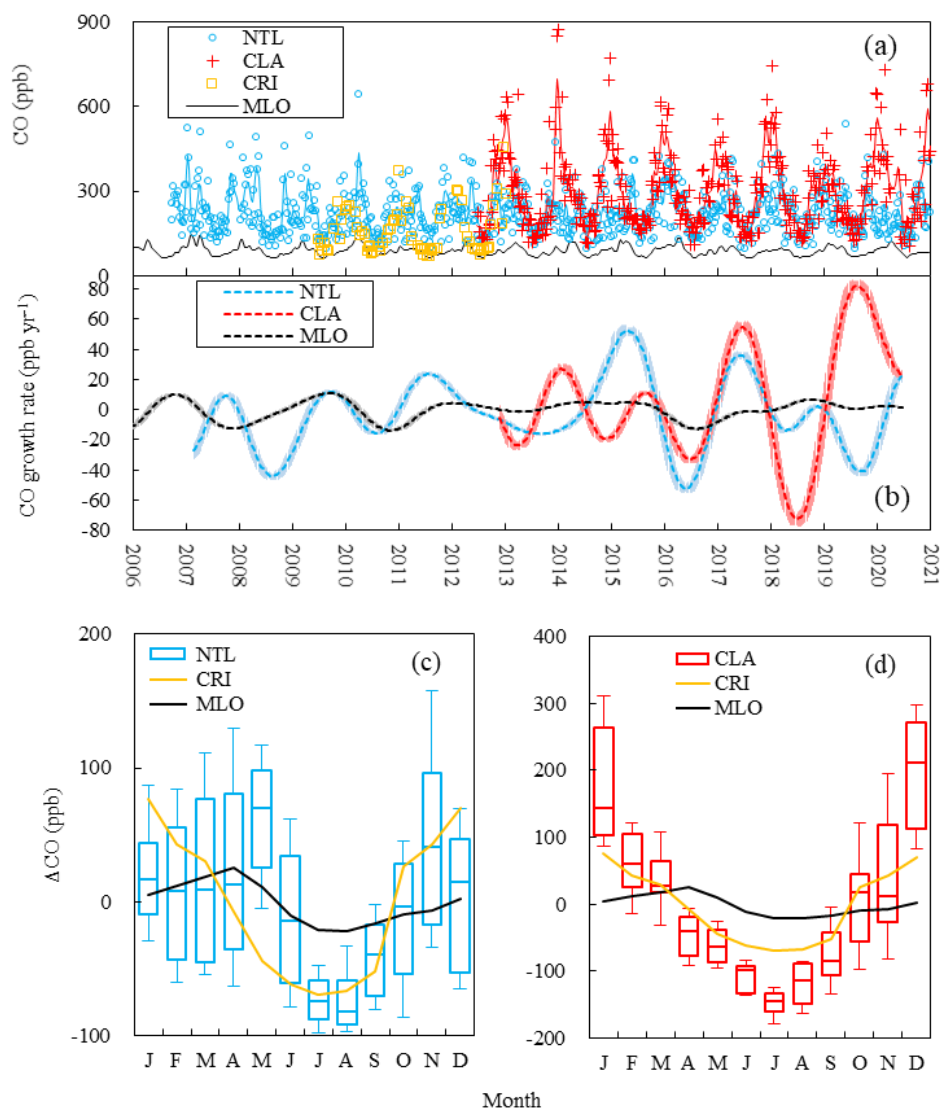
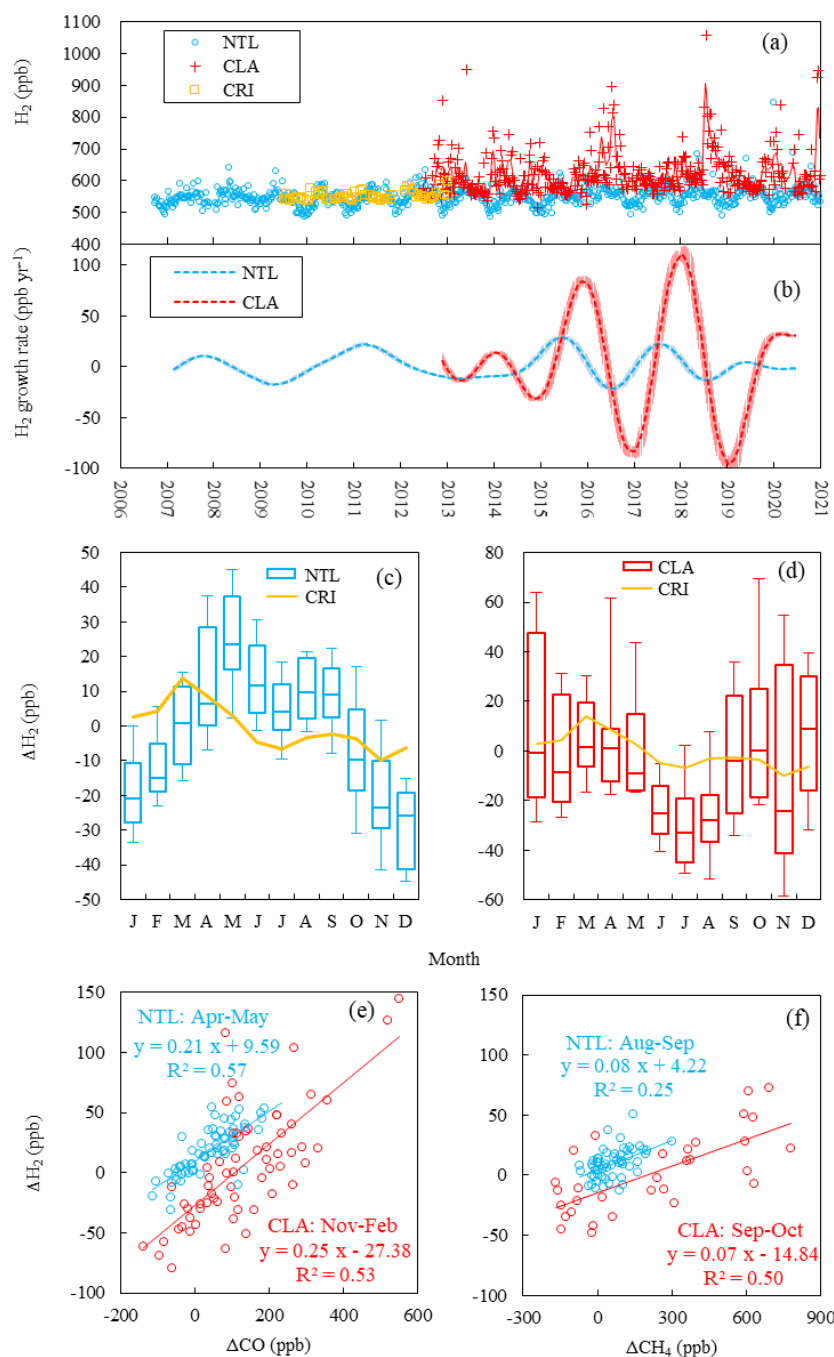


Figure 9. Time series of (a) measured values and (b) growth rate of the  $\text{CH}_4$  mole fraction at Nainital (NTL), Comilla (CLA), Cape Rama (CRI), and Mauna Loa (MLO) in 2006–2020, the seasonal variation in the  $\text{CH}_4$  mole fraction at (c) NTL and (d) CLA, and the relationship between the short-term component of  $\text{dCO}$  and  $\text{dCH}_4$  at (e) NTL and (f) CLA during January – March (JFM), April–June (AMJ), July–September (JAS) and October–December (OND).





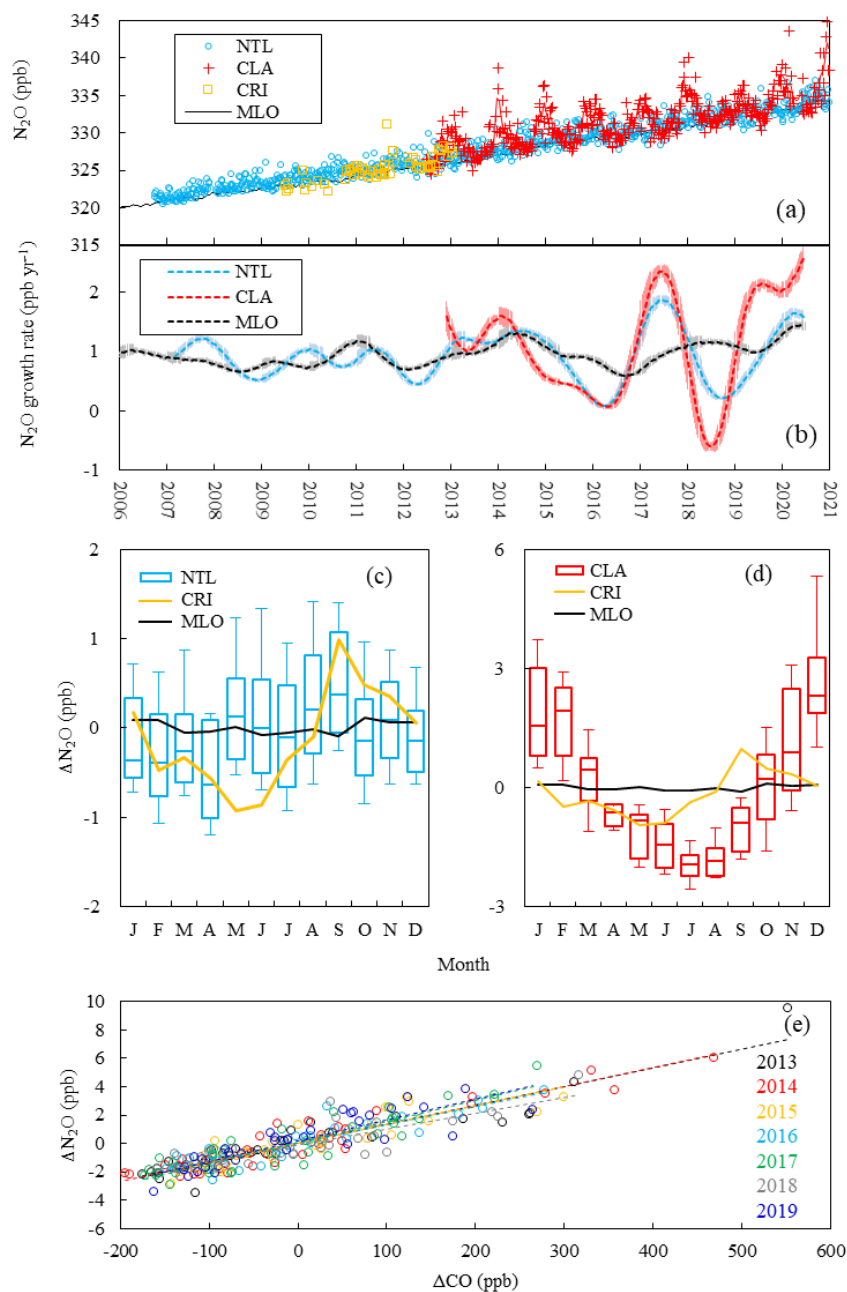
936  
 937 Figure 10. Time series of (a) measured values and (b) growth rates of CO mole fraction at Nainital (NTL), Comilla (CLA),  
 938 Cape Rama (CRI), and Mauna Loa (MLO) in 2006–2020, and the seasonal variation of CO mole fraction at (c) NTL and (d)  
 939 CLA.  
 940  
 941



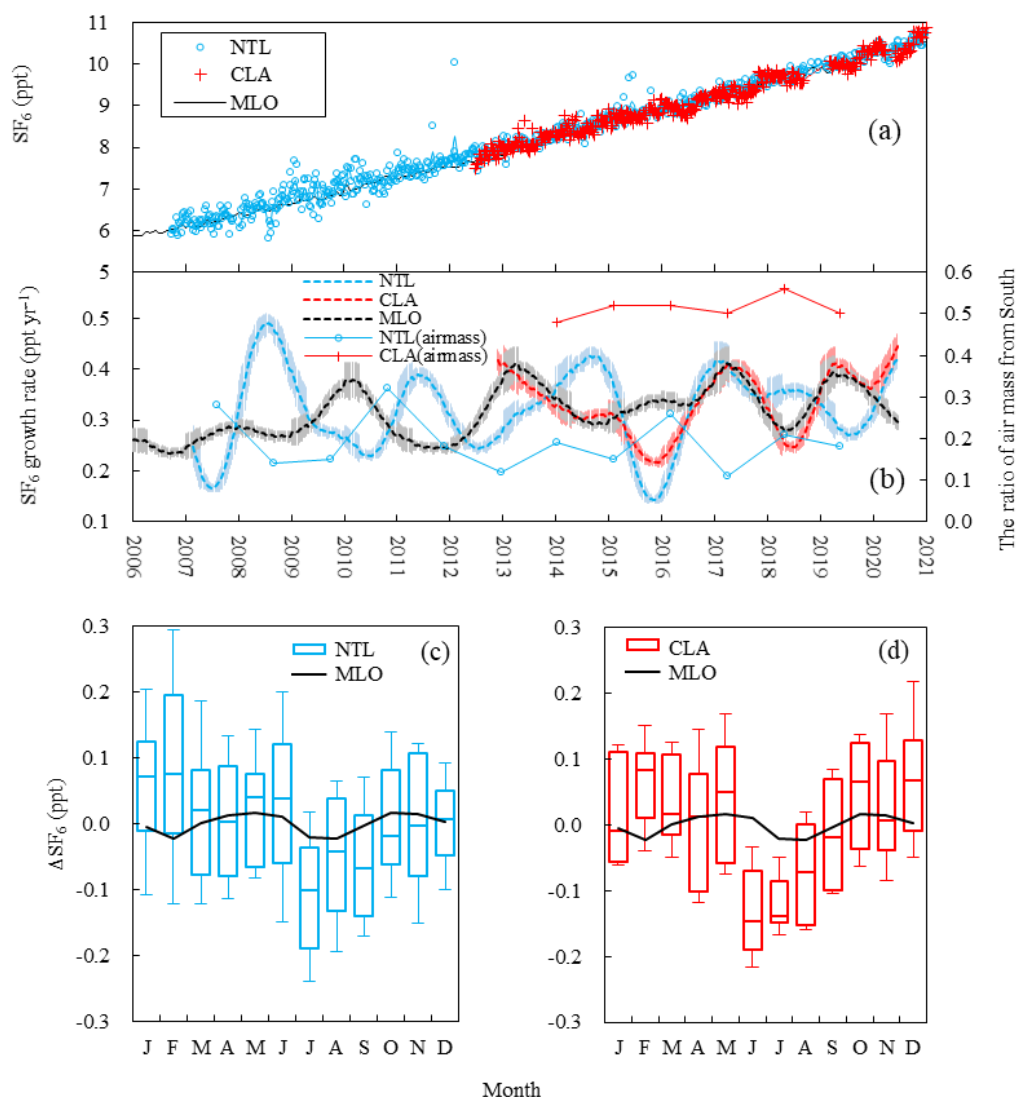
942

943

944 Figure 11. Time series of (a) measured values and (b) growth rate of the atmospheric  $H_2$  mole fraction at Nainital (NTL),  
 945 Comilla (CLA), and Cape Rama (CRI) in 2006–2020, seasonal variation in the  $H_2$  mole fraction at (c) NTL and (d) CLA,  
 946 and scatter plots for the relationship of (e)  $\Delta H_2$  and  $\Delta CO$  at NTL during April–May and at CLA during November–February  
 947 when biomass burning occurred frequently, and (f)  $\Delta H_2$  and  $\Delta CH_4$  at NTL during August–September and at CLA during  
 948 September–October when the maximum  $CH_4$  mole fraction was measured.



949  
 950 Figure 12. Time series of (a) measured values and (b) growth rates of the N<sub>2</sub>O mole fraction at Nainital (NTL), Comilla (CLA),  
 951 and Mauna Loa (MLO) in 2006–2020, seasonal variations in the N<sub>2</sub>O mole fraction at (c) NTL and (d) CLA, and (e) the  
 952 relationship between the ΔN<sub>2</sub>O and ΔCO at CLA in 2013–2019.  
 953



954  
 955  
 956 Figure 13. Time series of (a) measured values and (b) growth rates of the  $\text{SF}_6$  mole fraction at Nainital (NTL), Comilla  
 957 (CLA), and Mauna Loa (MLO) and the ratios of the air mass from south at NTL and CLA in 2006–2020, and seasonal  
 958 variations in the  $\text{SF}_6$  mole fraction at (c) NTL and (d) CLA.  
 959